GEOPHYSICS, VOL. 71, NO. 6 (NOVEMBER-DECEMBER 2006); P. R113–R130, 7 FIGS.
10.1190/1.2348763

Constrained Dix inversion

Zvi Koren and Igor Ravve

ABSTRACT

We propose a stable inversion method to create geologically constrained instantaneous velocities from a set of sparse, irregularly picked stacking- or rms-velocity functions in vertical time. The method is primarily designed for building initial velocity models for curved-ray time migration and initial macromodels for depth migration and tomography. It is mainly applicable in regions containing compacted sediments, in which the velocity gradually increases with depth and can be laterally varying. Inversion is done in four stages: establishing a global initial background-velocity trend, applying an explicit unconstrained inversion, performing a constrained least-squares inversion, and finally, fine gridding. The method can be applied to create a new velocity field (create mode) or to update an existing one (update mode). In the create mode, initially, the velocity trend is assumed an exponential, asymptotically bounded function, defined locally by three parameters at each lateral node and calculated from a reference datum surface. Velocity picks related to nonsediment rocks, such as salt flanks or basalt boundaries, require different trend functions and therefore are treated differently. In the update mode, the velocity trend is a background-velocity field, normally used for time or depth imaging. The unconstrained inversion results in a piecewise-constant, residual instantaneous velocity with respect to the velocity trend and is mainly used for regularizing the input data. The constrained inversion is performed individually for each rms-velocity function in vertical time, and the lateral and vertical continuities are controlled by the global velocity-trend function. A special damping technique suppresses vertical oscillations of the results. Finally, smoothing and gridding (interpolation) are done for the resulting instantaneous velocity to generate a regular, fine grid in space and time. This method leads to a stable and geologically plausible velocity model, even in cases of noisy input rms-velocity or residual rms-velocity data.

INTRODUCTION

Durbaum (1954) and Dix (1955) proposed to estimate interval velocities from picked rms, or stacking, velocities, and corresponding traveltimes by the well-known formula

$$U_n = \sqrt{\frac{V_{2,n}^2 t_n - V_{2,n-1}^2 t_{n-1}}{t_n - t_{n-1}}}, \tag{1}$$

where U_n is the local rms velocity over the time interval $\Delta t_n = t_n - t_{n-1}$, which approximates the actual interval velocity $V_n^{\text{int}} = \Delta z_n/\Delta t_n$, and Δz_n is the corresponding depth interval (Hubral and Krey, 1980). Parameters $V_{2,n-1}$ and $V_{2,n}$ are rms velocities at the top and bottom interfaces of the interval. Note that for any velocity distribution, $U_n \geq V_n^{\text{Int}}$ and the exact equality takes place only in the case of a constant velocity on the interval. Equation 1 (Dix transform) is the standard, unconstrained, explicit velocity inversion in which the instantaneous velocity $V_{0,n}$ is assumed piecewise constant, $V_{0,n} = U_n$, with discontinuities at the interfaces. The Dix transform can easily produce nonrealistic and highly oscillating velocities, even for relatively small variations in stacking or rms velocities.

We review several works related to the uncertainty of the classical Dix inversion. In these works, the authors use the term *interval velocity* instead of the more accurate term *local rms velocity* mentioned above. To be consistent with the cited works, the term *interval velocity* is also used in our review.

Uncertainty of interval velocity estimates was extensively studied by Hubral (1976), Hubral and Krey (1980), Toldi (1985), Thore et al. (2002), and other researchers. Hajnal and Sereda (1981) developed and analyzed the first-order-difference equation governing the uncertainty of the Dix inversion. They demonstrated that the uncertainty in the calculated interval velocity increases with depth and is inversely proportional to layer thickness:

$$\frac{\delta U_n}{\delta V_2} \approx \frac{2t}{\Delta t_n}, \tag{2}$$

where δU_n is the uncertainty of the interval velocity, δV_2 is the uncertainty of the rms velocity, t is the total traveltime at the midpoint of the interval, and Δt_n is the interval traveltime. The derivation is

Manuscript received by the Editor February 28, 2005; revised manuscript received March 27, 2006; published online November 3, 2006.
Paradigm Gav-Yam Center No. 3, 9 Shenkar Street, P. O. Box 2061, Herzliya B 46120, Israel. E-mail: zvi@paradigmgeo.com; igorr@paradigmgeo.com.

shown in Appendix A. The ratio $2t/\Delta t_n$ is an error-amplification factor: The uncertainty of the interval velocity obtained by the Dix inversion essentially exceeds the uncertainty of the rms velocity (i.e., $\delta U_n \gg \delta V_2$). Ursin (1981) studied the errors of direct and least-squares inversion schemes that estimate the interval velocity. In particular, he used a linear inverse scheme to determine the velocity function parameters in each layer. In this scheme, the difference between the measured and computed nonzero-offset traveltimes was minimized in the least-squares sense.

Landa et al. (1991) studied the uncertainties in the interval velocity and depth estimates in a general, layer-stripping approach; they accounted for local errors connected to the analyzed velocity layer and for global errors connected to the overburden model. The authors showed that the uncertainty in the interval velocity in a given layer depends primarily on uncertainties of the stacking velocities from the top and the bottom of the layer. There is a negative correlation between the velocity estimates in two successive layers (see Appendix A for details),

$$\frac{\partial U_{n+1}}{\partial U_n} = -\frac{\Delta z_n}{\Delta z_{n+1}}. \tag{3}$$

In other words, if there is a large error in the estimate for the nth layer, the error for the $n+1$th layer will be of the opposite sign and will partly compensate for the previous error. This leads to oscillations in the vertical velocity profile.

Seismic imaging is based on iterative improvement of the velocity field to obtain flat image gathers and a final image, which should also agree with the local geological assumptions. The seismic imaging solution is not unique. Many combinations of instantaneous velocity models can generate flat image gathers. It is therefore essential to constrain any inverted velocity field by the geologic rules relevant to the area of investigation. There is always a trade-off between the requirement for accuracy (fitting the data exactly) and the need for stability. Both the accuracy and the stability of the instantaneous velocity estimation are critical for seismic imaging, for which the Dix transform is normally used to obtain initial velocity models. Therefore, a number of implicit approaches have been developed such that a single erroneous value of stacking velocity does not easily corrupt the entire inversion. These methods are generally called *constrained velocity inversion* (Oldenburg et al., 1984; DuBose, 1988; Harlan, 1999; Zhang and Wang, 2003; Ren et al., 2004; Valenciano et al., 2004).

Vertical rms- (stacking-) velocity analysis is routinely used for velocity model building. The set of rms-velocity values picked along the vertical time axis at a given lateral location is stored as an rms-velocity function. From here forth, we refer to this set of values as an rms-velocity vertical function.

Harlan's (1999) algorithm finds a global solution for a set of vertical functions by applying the least-squares fit. A few noisy data points are largely ignored when contradicted by many neighboring values. Damping is applied to avoid unnecessary sharpness in the estimated instantaneous velocities. Ferguson and Stewart (1955) developed a linearization technique for a constrained inversion of P-S seismic data to give an S instantaneous-velocity estimate.

Several ray-based layer-stripping methods for velocity model determination had been studied. Gjoystdal and Ursin (1981) proposed a velocity-inversion approach using picked reflection times. Landa et al. (1988) described a method for determining velocity-depth model parameters by maximizing the coherency of the input traces measured along the calculated reflection time trajectories (coherency inversion) by applying the simplex method. A similar approach was applied by Sorin and Hanyga (1996). To speed up the iterative procedure for the seismic inversion with a poor initial guess, Druzhinin and Hanyga (1998) proposed a high-order perturbation method. This technique becomes an attractive alternative to iterative least-squares inversion to replace the linearization procedures when they become inconsistent.

A constrained instantaneous velocity is important as input for seismic inversion, which is a highly nonlinear problem. It is commonly solved iteratively by applying linear methods, such as seismic tomography (e.g., Goldin, 1986). Global tomography methods have been studied by many researchers. In these methods, traveltime errors along reflected rays are minimized to simultaneously find velocity-depth model parameters (Bishop et al., 1985; Williamson, 1990; Stork, 1992; Kosloff et al., 1996). The ray tracing in the tomography requires instantaneous velocity, and the success of the tomography depends strongly on the initial instantaneous velocity field, which is usually obtained by simplistic approximations.

Curved-ray time migration is now a standard procedure for time imaging. It requires an initial instantaneous velocity for 1D ray tracing. The initial instantaneous velocity is normally obtained by inverse Dix transform from picked rms velocities. It is essential to obtain a stable, geologically constrained inverted velocity with minimum oscillations.

In this study, we propose a stable and fast computational scheme for a constrained velocity inversion. The method can be applied to create a new velocity field (create mode) and to update an existing one (update mode). An important feature of the method is a characteristic velocity-trend function (background-guiding velocity model), initially approximated by a monotonously increasing and asymptotically bounded velocity function. In addition, the proposed method can be applied to update background velocities that are used in prestack seismic migrations (Deregowski, 1990). In this case, residual rms velocities are picked along the migrated image gathers, and they can be used, along with the background velocity, as the input for our constrained inversion. Here, the external background instantaneous velocity is used twice; it is a reference velocity and also a trend function for the inversion. We compute the rms velocity from the reference background instantaneous velocity and add the residual rms velocity to get the input for the inversion.

The velocity inversion is decoupled into two stages: explicit unconstrained and implicit constrained inversion. In the unconstrained inversion, we assume a piecewise-constant, residual instantaneous velocity that should be added to the background velocity. The residuals are constant values within the intervals between two successive picked points. To find the residuals, we assume that the unconstrained, inverted instantaneous velocity matches the input rms velocity exactly. We then use the unconstrained inverted velocities to regularize the input data on a uniform, coarse time grid, which is needed for the global constrained inversion.

The constrained inversion is a minimization problem. The inverted instantaneous velocity should not only match the given rms velocity; it should also be close to the trend model. A damping mechanism causes the results to behave in a stable, nonoscillatory fashion. The damping mechanism can either minimize the jumps of the inverted velocity gradient, or make these jumps close to the gradient jumps of the velocity trend. Following a widely used conventional approach, we also solve the inversion problem by the least-squares fit. The cost function includes three penalty terms: rms-velocity fit,

velocity-trend fit, and damping term. They all may have different weights in the cost function. The rms weight is responsible for the accuracy of the results. The trend weight controls lateral and vertical continuity, and the damping weight affects the stability of the inversion by suppressing the unwanted oscillations. For noisy data, the requirements for accuracy and stability, or continuity, may contradict each other. The optimum relation between the weights is a compromise. For a noisy input, the rms-velocity weight is automatically reduced to result in a stable and geologically plausible output. Most of the velocity inversion algorithms, both constrained and unconstrained, assume discontinuous, piecewise-constant instantaneous velocity, and the interval velocities are the degrees of freedom to be established (Dix, 1955; Taner and Koehler, 1969; Hubral and Krey, 1980; Grechka et al., 1996; Harlan, 1999; Ren et al., 2004). In our method, the instantaneous velocity within the compacted sediments is assumed continuous, and the degrees of freedom are instantaneous velocities at the interval ends (interfaces). Because n intervals correspond to $n + 1$ points, we have an extra degree of freedom compared to the classical approach. The problem, therefore, is underdetermined, and the additional inversion parameter allows us to control the results. Between the interfaces, we assume a linear variation of the instantaneous velocity in depth, which corresponds to an exponential velocity function in time.

The initial trend is an exponentially bounded velocity function that asymptotically approaches a predefined limit at large depth (Ravve and Koren, 2004, 2006a, 2006b). This function is characterized by three parameters: the instantaneous velocity, its vertical gradient at the datum surface (topography, sea bottom, or other known horizon representing the top of the sediment layers), and the asymptotic value. The parameters of the exponential velocity trend are established on a coarse lateral grid by global fitting to the rms-velocity data within predefined radii of influence.

For the inversion, we introduce a coarse, regular time grid with an origin at the datum horizon. Inversion is done individually for each vertical function; this results in the instantaneous-velocity-versus-time data at sparse and irregular lateral locations of the vertical functions. Finally, we apply a robust gridding algorithm, which interpolates and extrapolates the velocity field over the nodes of a fine, regular grid. Gridding is performed successively for slices, and each slice corresponds to a fixed node of the coarse time grid. Gridding is based on a minimum curvature method (Briggs, 1974), slightly modified to achieve better continuity.

A 2D synthetic data example of a salt body within a set of compacted sediments is used to demonstrate the method. A real field data set acquired above a fault-shadow area is then considered. The residual rms velocities were automatically picked, resulting in noisy, oscillating input data for the inversion. We show the ability of the constrained inversion to produce a geologically plausible, stable model from this type of data.

INITIAL TREND FUNCTION

The velocity-trend model can be given externally from a previous analysis or calculated internally from the rms-velocity data. In the latter case, the velocity-trend model is constructed on a coarse lateral grid. At each point of the lateral grid, the vertical variations of the instantaneous velocity are approximated by a monotonously increasing exponential, asymptotically bounded distribution (Ravve and Koren, 2004, 2006a):

$$V_0^{\exp}(z) = V_a + \Delta V \cdot \left[1 - \exp\left(-\frac{k_a z}{\Delta V}\right)\right], \quad \Delta V = V_\infty - V_a, \tag{4}$$

where $V_a(x,y)$ is the instantaneous velocity at the datum level, $k_a(x,y)$ is its vertical gradient at the same level, V_∞ is the asymptotic velocity at the infinite depth, and ΔV is the instantaneous-velocity range (see Figure 1). We assume that the asymptotic value V_∞ is approximately known from the physical properties of fully compacted sediments; however, the two other parameters, V_a and k_a, are to be established. Because the input rms velocities are given in time, we rearrange equation 4 to be instantaneous velocity versus one-way traveltime,

$$V_0^{\exp}(t) = \frac{V_a \cdot V_\infty}{V_a + \Delta V \cdot \exp(-k_a t \cdot V_\infty/\Delta V)}. \tag{5}$$

The trend parameters at each lateral, coarse-grid point are established by a least-squares fit. We request that the rms velocities computed from the exponential velocity-trend function $V_2^{\exp}$ should be as close as possible to the picked rms-velocity values V_2^{data}. Along the vertical direction, the rms velocity is defined by

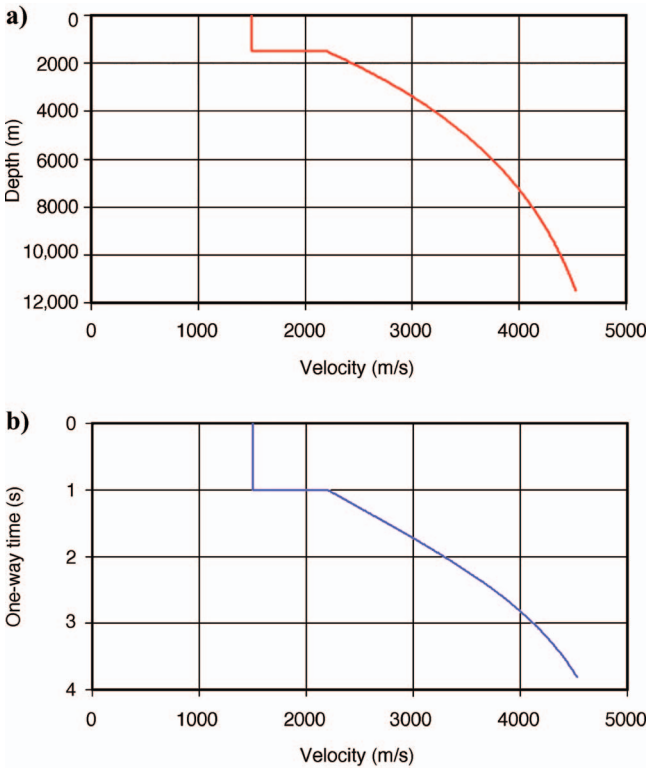

Figure 1. Exponential, asymptotically bounded velocity model: (a) instantaneous velocity versus depth, (b) instantaneous velocity versus one-way traveltime. The sea bottom depth is 1500 m; the marine velocity is 1500 m/s. Parameters of the exponential velocity distribution are V_a = 2200 m/s, k_a = 0.5 s^{-1}, and V_∞ = 5000 m/s.

$$V_2(t) = \sqrt{\frac{1}{t} \cdot \int_0^t V_0^2(\tau) d\tau} \equiv \sqrt{\frac{W(t)}{t}}, \qquad (6)$$

where W is a hyperbolic parameter defined as $W = \int_0^t V_0^2(\tau) d\tau$. For the exponential distribution (Ravve and Koren, 2004, 2006a),

$$W^{\exp}(t) = \frac{\Delta V \cdot V_\infty}{k_o} \cdot \ln \frac{S}{V_\infty} - \frac{V_a \cdot \Delta V^2}{k_o} \cdot \frac{\lambda - 1}{S},$$
$$\lambda \equiv \exp(k_o t \cdot V_\infty / \Delta V), \quad S \equiv V_a \cdot \lambda + \Delta V,$$
$$\Delta V = V_\infty - V_a. \qquad (7)$$

Thus, the rms velocity V_2 of the exponential distribution is a function of the two parameters, V_a and k_a, and of the time $V_2^{\exp}(V_a, k_a, t)$.

We introduce a predefined radius of influence R. For any coarse-grid point, all vertical functions that are laterally within the given radius, $d \le R$, will affect the trend parameters. However, the vertical functions will have different weights. The weight decreases as the distance between the grid point and the vertical function increases. The maximum weight is unity and corresponds to a vanishing distance. We propose the following weighting function:

$$w_{ij}^L = \exp(-\alpha d_{ij}^2 / R^2) \quad \text{for} \quad d_{ij} \le R,$$
$$w_{ij}^L = 0 \quad \text{for} \quad d_{ij} > R, \qquad (8)$$

where superscript L means lateral. In this equation, i is the index of the vertical function, and j is the index of the grid node where the velocity-trend parameters are being estimated. For the limiting case $d = R$, we desire a preset weight $w^L = \xi$, where ξ is a given small value, say one percent, $\xi = 10^{-2}$. This leads to $\alpha = -\ln \xi$ in equation 8. Obviously, a larger radius of influence improves stability but decreases accuracy of the inversion results.

In addition to the lateral weights w_{ij}^L, there are also vertical weights w_n^V. The lateral weights are the same for all points of each specific vertical function. The vertical weights usually decrease with traveltime. The misfit function becomes

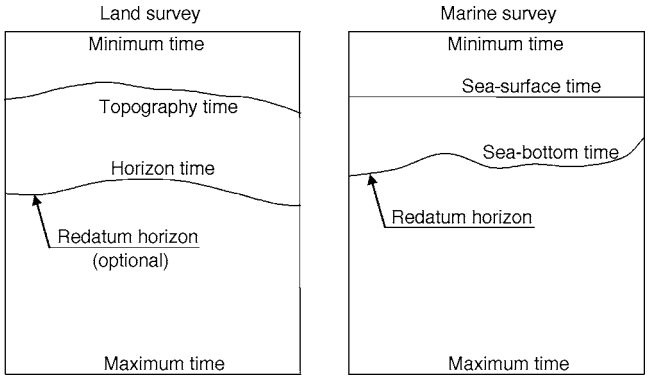

Figure 2. Redatuming scheme for a land and a marine survey. After redatuming, the input rms velocity is measured from a reference horizon. This horizon is also the origin of the coarse time grid used in the constrained inversion.

$$A_j(V_a, k_a) = \frac{1}{2} \sum_{i=0}^{M_j - 1} w_{ij}^L \sum_{n=0}^{N_i} w_n^V [V_2^{\exp}(V_{a,j}, k_{a,j}, t_{in}) - V_{2,in}^{\text{data}}]^2 \to \min, \qquad (9)$$

where the inner sum stands for all $N_i + 1$ picked nodes of the fixed vertical function i, and the outer sum accumulates all M_j vertical functions within the radius of influence around lateral node j. The necessary condition for a local minimum requires that the two partial derivatives $\partial A_j / \partial V_a$ and $\partial A_j / \partial k_a$ vanish. This leads to a nonlinear set with two unknown variables, and we solve it by applying an iterative procedure. The solution technique is presented in Appendix B. Thus, the trend parameters V_a and k_a are computed at each node of the coarse grid by global fitting of the exponential model to the data. The top velocity and its gradient are then further interpolated to a fine grid, and in particular, they are established at the lateral locations of the vertical functions.

It is important to note that the calculated internal-velocity trend is geologically adequate only for compacted sediment layers, possibly for layers with small anomalies. The exponential velocity model represents the real physical behavior of the velocity profile, in which the velocity gradually increases with depth and approaches a limiting value at large depth. Conventional velocity-versus-depth models [linear velocity and classical unbounded exponent (Slotnick, 1936, 1959); linear slowness (Al-Chalabi, 1997a; Faust, 1951, 1953) with different power indices, parabolic (Houston, 1939; Al-Chalabi, 1997b); etc.] all suffer from the same disadvantage: they are unbounded at large depth. Among the family of monotonously increasing and bounded models, we found the exponential asymptotic model to be the most simple and adequate. In the case of strong velocity variations, such as in salt domes, basalts, or high-velocity carbonate rocks, the velocity trend will bias the results of the inversion in a wrong fashion. Therefore, when the parameters of the internal trend are being calculated, we filter out the picks on and below the first strong velocity anomaly and assume that the sediments extend to the maximum depth considered. The velocity anomalies will be still approximately found by the inversion. To treat more accurately the velocity anomalies in the case of rapid velocity change or discontinuity of the instantaneous velocity or a decreasing-velocity-with-depth trend, an external background trend is needed. This function is specified numerically and accounts for the anomalies. It can be obtained from a previous run of the proposed inversion or from a more accurate ray-based tomographic inversion. The technique of inversion with an external trend function is presented in Appendix H.

REDATUMING

Because the velocity trend starts from a reference horizon, a redatum procedure should be performed before calculating the trend. At the reference horizon, the rms velocity V_2^H and the traveltime t_H are specified. For a marine survey, the rms velocity is normally the water velocity. We drop out all picked points whose traveltime does not exceed the horizon time. For data points below the horizon, the redatum formula is defined by

$$V_{2,n}^{\text{new}} = \sqrt{\frac{V_{2,n}^{2\ \text{old}} \cdot t_n^{\text{old}} - V_{2,H}^2 \cdot t_H}{t_n^{\text{old}} - t_H}}, \quad t_n^{\text{new}} = t_n^{\text{old}} - t_H. \qquad (10)$$

The redatum horizon is shown in Figure 2 for land and marine surveys.

EXPLICIT, UNCONSTRAINED VELOCITY INVERSION

The explicit, unconstrained velocity inversion described here follows the velocity-trend function and is defined by a set of piecewise-constant residuals to be found. It differs from the standard, unconstrained Dix (1955) inversion, which does not require a trend but leads to noisy and highly oscillating results.

We distinguish two inversion modes: create and update. In both cases, the input data are vertical functions of rms velocities at sparse, irregular, lateral locations. The picked points in the vertical direction are also sparse. In the create mode, the rms or stacking velocities $V_{2,k}^{\text{data}}$ are picked along unmigrated gathers (or inverse, NMO-migrated gathers). In the update mode, the picked values are residuals of the rms velocity $\Delta V_{2,k}$, and the rms velocities are calculated. First, the background instantaneous velocity used for the migration is transformed to rms velocity versus time. Second, we add the picked residual rms velocities in time to the background rms-velocity model and get the vertical function at the sparse picked points:

$$V_{2,k}^{\text{data}} = V_{2,k}^{\text{trend}} + \Delta V_{2,k}, \tag{11}$$

where the rms velocities and residuals are measured from the earth's surface. Third, we apply the redatum procedure described above. Fourth, we proceed with the unconstrained inversion described below in this section. Fifth, we use the unconstrained inversion results for regularization of the input rms data on a coarse time grid.

The unconstrained velocity inversion is based on an assumption that, between two successive picked points, the instantaneous velocity follows the velocity-trend function with a constant, residual instantaneous velocity,

$$V_{0,k}^{\text{data}}(t) = V_{0,k}^{\text{trend}}(t) + \Delta V_{0,k}, \tag{12}$$

where k is the index of the interval between two picked points. The velocity-trend function in equation 12 can be external or internal. The unknown residual $\Delta V_{0,k}$ is calculated by equation 13 (see Appendix C for details)

$$\Delta V_{0,k} = \sqrt{(U_k^{\text{data}})^2 - (U_k^{\text{trend}})^2 + (V_{\text{int},k}^{\text{trend}})^2} - V_{\text{int},k}^{\text{trend}}, \tag{13}$$

where U_k^{data} and U_k^{trend} are local rms velocities on the interval k between two picked points for the input vertical function and the velocity trend, respectively. Parameter $V_{\text{int},k}^{\text{trend}}$ is the interval (local average) velocity of the trend between the picked points. After we obtain the constant residuals $\Delta V_{0,k}$, the instantaneous velocity becomes a known function (equation 12). Note that at the endpoints of the original interval t_{k-1} and t_k, the unconstrained inverted velocity fits the rms data exactly. To calculate the interval (local average) and the local rms velocity of the trend, we use the trend data on a fine time grid.

CONSTRAINED VELOCITY INVERSION

We perform the inversion for each vertical function individually, assuming a locally varying 1D model. Following a conventional approach, we solve the inversion problem by the least-squares fit (e.g., Tarantola, 1987; Menke, 1989). The primary drawback of the method is a lack of robustness, i.e., strong sensitivity to outliers (a small number of large errors) in the data set. Another inevitable problem of the least-squares inversion is nonuniqueness: More than one solution will satisfy the observation within a prescribed error, and different models may satisfy the mean-squares error equally well (e.g., Lines and Treitel, 1985). In this study, we exploit the velocity-trend model and the damping technique to reduce the sensitivity of inversion to noise. Increase of weights for trend function and damping mechanism will necessarily lead to a smooth, stable, and unique solution and will suppress any anomalous rms-velocity picks. However, setting these weights too high will suppress even the reliable data. In case of an excessive trend weight, the resulting solution will almost coincide with the trend. In the case of an excessive damping weight, the solution will produce a nearly linear distribution of velocity versus depth within the whole depth range. The optimum level of suppression is a trade-off between the desired accuracy and stability, which requires an informal, ad hoc choice of the weights through trial and error (DuBose, 1988).

Regularization in time

Recall that the picked points are irregular not only laterally but also in time. We apply regularization in time by introducing a regular, coarse time grid. This will facilitate the lateral gridding procedure that follows the multiple 1D inversion of the vertical functions. Gridding is performed successively by slices, whereby each slice corresponds to a fixed time measured from the datum.

At this point, the unconstrained inversion is already performed. Equation 12 represents a continuous function $V_0^{\text{data}}(t)$ that matches exactly the input rms-velocity data at the picked points. In addition, $V_0^{\text{data}}(t)$ follows the velocity trend. We apply the standard interpolation formula to obtain the rms velocity $V_{2,n}^{\text{data}}$ at any point n between the picked points $k-1$ and k,

$$(V_{2,n}^{\text{data}})^2 \cdot t_n = (V_{2,k-1}^{\text{data}})^2 \cdot t_{k-1} + \int_{t_{k-1}}^{t_n} [V_{0,k}^{\text{data}}(\tau)]^2 d\tau,$$

$$V_{0,k}^{\text{data}}(\tau) = V_{0,k}^{\text{trend}}(\tau) + \Delta V_{0,k}, \quad t_{k-1} \le t_n \le t_k. \tag{14}$$

This interpolation is applied to regularize the input rms velocity for a uniform, coarse time grid.

Cost function

To reduce the sensitivity of the inversion to data noise, we construct a cost function that includes three components. The rms-velocity misfit (data misfit) is only one of them. The two others, the velocity-trend-model misfit and the antioscillatory damping energy, improve the robustness and stability of the method. The optimum values of the parameters (instantaneous velocities at the nodes of the coarse time grid) minimize the cost function F:

$$F = \underbrace{B}_{\text{Data misfit}} + \underbrace{C}_{\text{Trend misfit}} + \underbrace{D}_{\text{Damping energy}} \rightarrow \min. \tag{15}$$

Next, we derive the three components of the cost function in equation 15, referred to also as a variation-energy function.

Data misfit

Suppose that the vertical rms-velocity function includes $N + 1$ equally spaced nodes; thus, there are N intervals. The unknown values are nodal instantaneous velocities: $V_{0,0}, V_{0,1}, \ldots, V_{0,N}$. Consequently, we have $N + 1$ degrees of freedom to be established. Between the coarse grid nodes, we assume a linear variation of the instantaneous velocity in depth. Let $V_{0,n-1}$ and $V_{0,n}$ be the inverted instantaneous velocities at the top and bottom interface of the coarse interval $\Delta t_n = t_n - t_{n-1}$. For the linear velocity distribution in depth, the inverted, local rms velocity U_n^{lin} becomes a function of the two interface velocities related to that interval (see Appendix D for details):

$$U_n^{\text{lin}}(V_{0,n-1}, V_{0,n}) = \sqrt{\frac{V_{0,n}^2 - V_{0,n-1}^2}{2\ln(V_{0,n}/V_{0,n-1})}}. \quad (16)$$

The inverted, local rms velocities for the intervals U_n^{lin} should fit the local rms-velocity data U_n^{data}. The data-misfit function is the first component of the variation energy (equation 15). Assume that in the vertical direction, the nodes are enumerated from zero, the intervals are enumerated from unity, and interval n connects nodes $n - 1$ and n. Summing the data misfit over the intervals, we obtain

$$B = \frac{1}{2}\sum_{n=1}^{N} \Delta t_n \cdot w_n^{\text{rms}}[U_n^{\text{lin}}(V_{0,n-1}, V_{0,n}) - U_n^{\text{data}}]^2, \quad (17)$$

where w_n^{rms} are weights of the data misfit on the intervals. These weights may be data dependent (lesser weights for noisy data and vice versa). In the case of a noisy input leading to unstable (oscillating) results, we reduce the weights of the rms-velocity fit as compared to the weights of the trend function and damping mechanism, and we rerun the inversion. Note that only the ratio between the different weights is important.

Geophysical inverse problems are generally not well-posed. Many of these problems are overdetermined, i.e., the number of data points exceeds the number of model parameters (Lines and Treitel, 1984). Normally, the number of picked traveltimes is the upper limit for the model parameters that one can safely invert (Vesnaver and Bohm, 2000). The approach we propose in this study is an exception: it is an underdetermined problem. We have $N + 1$ unknown instantaneous velocities at the nodes and N observed local rms velocities (data) on the intervals. However, because the data alone leads to an underdetermined system, either the trend-misfit term or the damping-energy term is a must in the cost function. We include both of them. The weights of the velocity trend and the damping weight can not both be negligibly small as compared to the weights of the data fit because this will lead to an ill-conditioned equation set with an unstable solution.

Trend misfit

The inverted instantaneous-velocity function should be as close as possible to the velocity trend. The trend-misfit function can be defined as the L_2-norm of the difference between the instantaneous velocity model and the trend model:

$$C = \frac{1}{2}\sum_{n=1}^{N} \int_0^{\Delta t_n} w_n^{\text{trend}}[V_{0,n}^{\text{lin}}(\tau) - V_0^{\text{trend}}(t_{n-1} + \tau)]^2 d\tau \rightarrow \min, \quad (18)$$

where summation is done over the intervals and w_n^{trend} is the weight of the nth vertical interval. Normally, these weights decrease with traveltime. For the linear instantaneous velocity versus depth, velocity versus time reads (see Appendix D)

$$V_{0,n}^{\text{lin}}(\tau) = V_{0,n-1}^{1-\tau/\Delta t_n} \cdot V_{0,n}^{\tau/\Delta t_n}, \quad 0 \le \tau \le \Delta t_n. \quad (19)$$

In the case of an internal (initial) exponential trend, the instantaneous velocity $V_0^{\text{trend}}(t)$ is given by equation 5. Otherwise, it is an external function specified at the nodes of the fine grid (normally, with the standard two-way resolution of 4 ms), and we consider it as a given, continuous function of time.

Antioscillatory damping mechanism

The interval velocities obtained by Dix inversion are subjected to essential uncertainties. To suppress the unwanted vertical oscillations of the inverted velocity, we propose a special stabilization technique, implemented as a damping term in the cost function. Recall that the vertical gradient of the inverted velocity is assumed piecewise-constant, with the discontinuities of the gradient at the nodal points.

We propose two kinds of damping mechanisms:

- *Absolute damping mechanism* that suppresses any gradient jumps (usually applied with the internal trend).
- *Damping mechanism following trend* that allows gradient jumps similar to the jumps of the trend model (usually applied with the external trend). This damping technique keeps a minimum discrepancy between the gradient jumps of the model and the velocity trend.

Technical details related to damping terms are explained in Appendix E.

Initial guess

To get an initial guess for the velocity function, we apply the unconstrained Dix-inversion formula (equation 1) resulting in piecewise-constant instantaneous velocities with discontinuities at the interfaces. Recall that interval n stretches between the interfaces $n - 1$ and n. To get the velocities $V_{0,n}$ at the interfaces, we average their values above and below the interface:

$$V_{0,n} = \frac{U_n + U_{n+1}}{2}. \quad (20)$$

The exceptions are, of course, the first interface (datum) and the last interface, where no averaging is needed.

Minimizing the cost function

At the minimum point, all partial derivatives of the variation-energy function with respect to the model parameters $V_{0,n}$ vanish. Equation 15 yields a nonlinear set of $N + 1$ equations with $N + 1$ variables: $\partial F/\partial V_{0,n} = 0$. The data-misfit and the trend-misfit terms

present a sum of items, where each item is related to a definite interval and depends on two nodal velocities at the ends of this interval. Therefore, these terms result in a tridiagonal matrix of second derivatives (Hessian matrix) $\partial^2 F/(\partial V_{0,n}\partial V_{0,m})$. The damping term is a sum of the items, where each item is related to a definite joint and depends on three nodal velocities: that at the joint and two other velocities at the nodes immediately before and after the joint. This term makes the resulting Hessian matrix pentadiagonal. We use a special direct solver for a symmetric pentadiagonal matrix, and the computations are very fast. The technique of solution for the nonlinear set is based on the Newton method and is presented in Appendix F. Two or three iterations usually suffice for convergence.

Besides the Newton method, one of the most common algorithms used to find local minima in multidimensions is the conjugate-gradient method (Hestens and Stiefel, 1952) and its variations. The method was developed for the solution of sparse systems and is widely used to solve large geophysical inverse problems (e.g., VanDecar and Snieder, 1994; Kosloff et al., 1996). Its advantage is that the method does not require the knowledge of the Hessian matrix; however, it requires about N iterations to converge, where N is the amount of model parameters (Press et al., 1999). For the problem that we solve, the maximum two-way traveltime is usually a few seconds, and the resolution of the coarse time grid is $\sim$0.1 s, so that N may vary from 60 to 100 per vertical function. The Newton method requires the Hessian matrix of the variation energy, but this matrix is symmetric and either tridiagonal (no damping term in the cost function) or pentadiagonal (with a damping term). Thus, the second derivative consists of only two or three vectors (diagonals); therefore, we found this approach efficient.

GENERATION OF OUTPUT ON A REGULAR MESH

As a result of the inversion, the instantaneous velocities are obtained at lateral locations of vertical functions on a regular, coarse time grid. A special gridding procedure is needed to get a regular fine grid of the instantaneous velocities. Because the time grid is the same for all vertical functions (with respect to the datum surface), we apply the gridding procedure successively for all time slices. For each slice, the traveltime is fixed and a 2D problem is considered. There is a set of control points at the locations of vertical functions, and there are also trend values at the other grid nodes. The weight of trend values is now very small, and the weight of control values is large but still finite and not extremely large. Larger weight of the control points leads to a better accuracy of the result at the control points, but this can yield a worse lateral continuity and vice versa. The optimum weight is a compromise.

Different gridding algorithms exist that take the observed values at the control points to define the value of a continuous function of the two space variables. Bhattacharyya (1969) proposed to use a bicubic spline interpolation. Briggs (1974) proposed to solve a biharmonic equation to result in a surface of minimum curvature. Physically, this surface models static bending of a thin, elastic plate (Timoshenko and Woinowsky-Krieger, 1968). Smith and Wessel (1990) introduced a tension term into the minimum-curvature equation to suppress oscillations and to avoid extraneous inflection points.

To find the nodal velocities, we apply a slightly modified Briggs (1974) approach, relaxing the requirement of exact data fit at the observation (control) points (e.g., Lancaster and Salkauskas, 1986). For this, we consider static bending of a thin, rectangular plate with free edges. The plate rests on soft springs (trend points) and stiff springs (control points). The springs are unstretched when the bending displacements at their locations are equal to the given control or trend values. The weights are rigidities of control and trend springs related to the plate stiffness. The springs are not necessarily located at the nodes. The problem is solved by the finite-element method. Each node has three degrees of freedom: velocity and its derivatives in two lateral directions. The stiffness matrix is symmetric and narrowband. For 2D single line, a beam with free ends resting on springs is calculated instead of a plate. The technique of gridding is explained in Appendix G.

BACKWARD REDATUMING

After the gridding, we perform backward redatuming. The values of inverted instantaneous velocities are correct, but time shift is needed because the origin of the coarse time grid corresponds to the laterally varying datum surface. Therefore, the datum time (e.g., sea bottom in marine data) should be added. Above the datum, the instantaneous velocities are known before the inversion. Finally, we interpolate vertically for the fine time grid, assuming linear variations of the instantaneous velocity in depth between the nodes of the coarse time grid.

SYNTHETIC EXAMPLE

A synthetic example of the velocity inversion is shown in Figure 3. The model consists of a laterally varying sea-bottom profile, thick sediment layers, and a salt body within. Finite-difference modeling (Tal-Ezer et al., 1987) was used to generate synthetic data of 750 common midpoints (CMPs) with a 25-m interval. The true instantaneous-velocity model scaled from depth is shown in Figure 3a. Figure 3b and c demonstrate the undamped and damped (with the

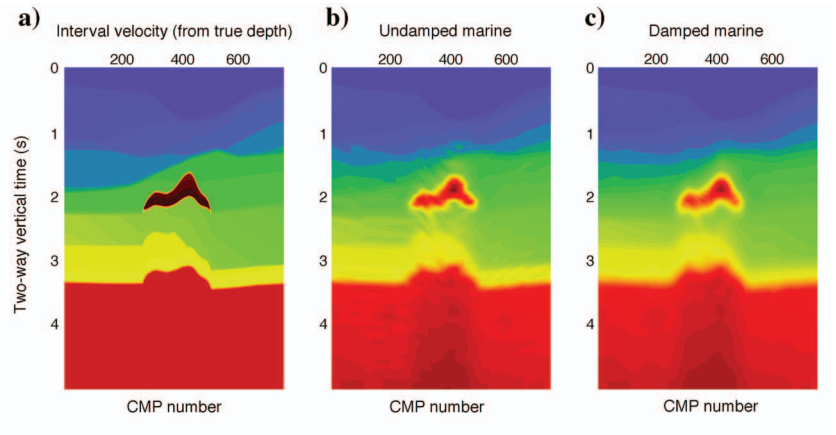

Figure 3. (a) True instantaneous-velocity model (scaled from depth), 750 CMPs with a 25-m interval. The two-way traveltime range is 5 s. (b) Noisy result of the constrained velocity inversion — no damping involved. The unwanted vertical oscillations of the instantaneous velocity are present. (c) Stable damped result of velocity inversion. Range of the inverted instantaneous velocity: minimum, 1.5 km/s; maximum, 4.8 km/s.

weight $w^{damp} = 2$) results of the inversion, respectively. The unwanted vertical oscillations of the instantaneous velocity are clearly seen in Figure 3b. The minimum instantaneous velocity is 1.5 km/s, and the maximum is 4.8 km/s.

A total of 75 rms-velocity vertical functions were automatically picked and used as input for the inversion, and the instantaneous velocity was obtained (Figure 3c). Figure 4a shows the rms-velocity section obtained from the inverted instantaneous velocity (by forward Dix transform). The minimum rms velocity is 1.5 km/s, and the maximum is 3.6 km/s. The marine (sea bottom) horizon was used as a redatum surface. Next, we consider a representative vertical function (CMP#321) that involves reflections from the salt body. The dashed vertical line in Figure 4a shows the selected location. Figure 4b shows the results of the inversion for this specific location: the instantaneous velocity (red solid line) and the rms velocity obtained by forward Dix transform from the inverted instantaneous velocity (red dashed line). The pink crosses are rms-velocity picks. The inverted rms velocity does not necessarily pass through the picked points, although it is very close. There is no exact match between the rms input data and the results. It is only the best fit in a least-squares sense. Figure 4c shows the CMP gather for that location. The pink lines along the input CMP gathers are hyperbolas corresponding to the picked rms velocities.

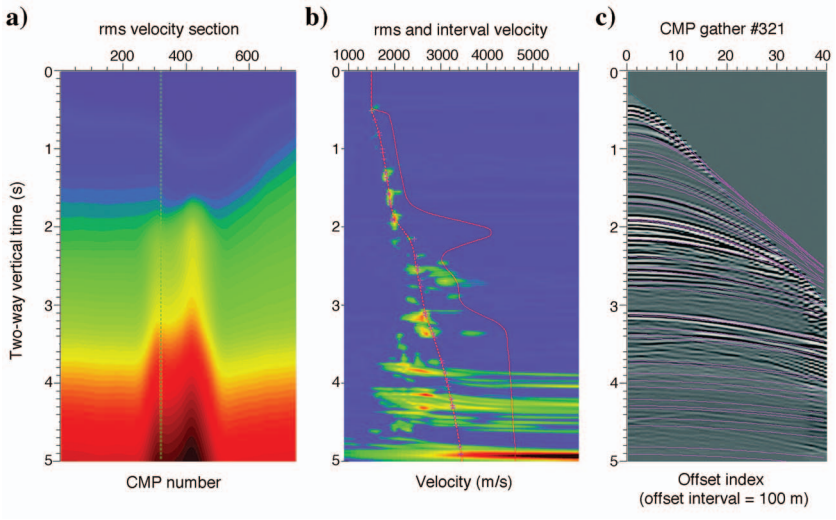

Figure 4. (a) The rms-velocity section obtained after inversion. Range of the rms velocity: minimum, 1.5 km/s; maximum, 3.6 km/s. (b) Semblance, vertical function, and result of inversion for CMP#321. The instantaneous velocity is shown by red solid line, and the rms velocity obtained by forward Dix transform from the inverted instantaneous velocity is shown by red dashed line. The pink crosses are rms-velocity picks. Residual rms-velocity scale range is -610 m/s (-2000 ft/s) $\le \Delta V_2 \le +610$ m/s ($+2000$ ft/s). Instantaneous- and rms-velocity scale range is: 1520 m/s (5000 ft/s) $\le \{V_0, V_2\} \le 4570$ m/s (15000 ft/s). (c) CMP gather #321. The pink lines along the input CMP gathers are hyperbolae corresponding to the picked rms velocities.

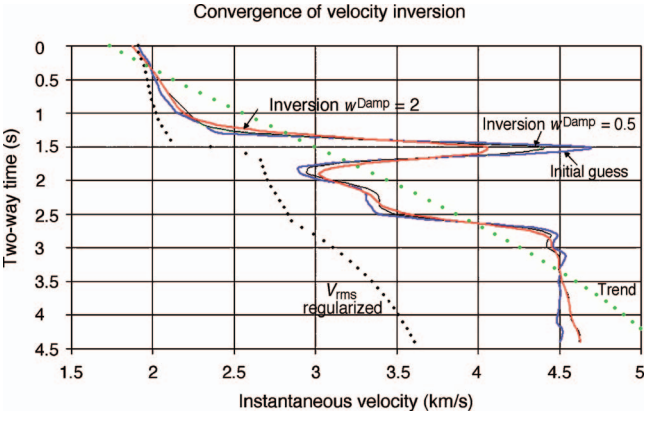

Figure 5. Convergence of the constrained Dix inversion. The two-way time is measured from the reference datum. Black dots are regularized input rms velocities on the coarse time grid. Green dots show internal trend — an exponential, asymptotically bounded velocity function. The blue solid line is the initial guess for the constrained velocity inversion. The black thin line is the result of the inversion with the damping weight $w^{damp} = 0.5$, and red thick line is the result with $w^{damp} = 2$.

Figure 5 illustrates the convergence of the iterative procedure. The green points show the internal exponential velocity trend. The black points are the input rms velocities measured from the datum surface (in this case, the sea bottom) and regularized on a coarse time grid (45 nodes, with two-way time interval $\Delta t = 0.1$ s). The thin blue line is the initial guess for the instantaneous velocity obtained by the standard Dix inversion with further averaging of the discontinuities. Two iterations of the Newton method were needed to achieve convergence, but the velocities after the first iteration almost coincide with the final inversion results, and these two lines on the plot look identical. We see only the final result, shown by the thin black line. The weight of the data misfit was 1, the trend weight was 0.25, and the damping weight was 0.5. The solid red line shows the solution for an increased damping weight $w^{damp} = 2$. For large traveltimes, between 3 and 4.4 s, the resulting solution tends toward higher velocities than those of the initial guess. This is the effect of the exponential velocity trend, which assumes that the sediment velocity increases with depth. The user can control this effect and even switch it off.

REAL DATA EXAMPLE

The velocity inversion was performed in update mode for real data acquired above a fault-shadow region. The data include 270 vertical functions for residual rms velocities ΔV_2^{data} at 270 CMPs. Figure 6a shows the background-velocity field and the result of the prestack time migration (PSTM). In Figure 6b, we present the result of the constrained velocity inversion for the representative CMP #9763. We show the instantaneous-velocity trend $V_0^{trend}(t)$ (black solid line); the rms velocity $V_2^{trend}(t)$ transformed from the velocity trend (black dash line); the inverted instantaneous velocity V_0^{inv} (turquoise solid line); the rms of the inverted velocity V_2^{inv} (turquoise dash line); the resulting residual rms velocity ΔV_2^{inv} (pale blue solid line), which is the difference between the rms of the inverted velocity and the rms of the background-velocity trend, $\Delta V_2^{inv} = V_2^{inv} - V_2^{trend}$; and the input residual rms velocity $\Delta V_{2,k}^{data}$ (pink crosses). As we see, the graph of the resulting residual $\Delta V_2^{inv}(t)$ does not pass exactly through the picked points $\Delta V_{2,k}^{data}$ but is close to the data.

Figure 6c shows the PSTM image gather for this location. The pink lines in Figure 6c represent time moveouts, $t_0 + \Delta t$ versus offset h for the residual rms velocity $\Delta V_{2,k}^{\text{data}}$ picked in Figure 6b:

$$\Delta t(h) = -\frac{h^2}{t_0 \cdot (V_2^{\text{trend}})^3} \cdot \Delta V_2^{\text{data}}. \qquad (21)$$

Figure 7a shows the background-velocity trend $V_0^{\text{trend}}(t)$ for all CMPs. Figure 7b shows the input residual rms velocity which was obtained by an automatic picking procedure (Swan, 2001). The result of the automatic picking is rather noisy, and the range of the residual rms velocity is -240 m/s (800 ft/s) $\le \Delta V_2^{\text{data}} \le 430$ m/s (1400 ft/s). Figure 7c demonstrates the ability of the constrained inversion to produce a geologically plausible and stable result even for this type of data. The weight of the data (rms velocity) misfit was 1, the weight of the trend misfit was 0.25, and that of the absolute damping was 0.5. Figure 7d shows the result of the unconstrained inversion, which is somewhat noisy. The color scale on the right side of Figure 7 is related to velocities (Figure 7a, c, and d). For the residual rms velocities in Figure 7b, dark blue corresponds to the minimum value -240 m/s, while red corresponds to the maximum value +430 m/s.

This example reflects the attractiveness of the implementation of the constrained inversion in a production environment. It enables the use of noisy, automatic picking output as an input for velocity updating, without the need for intensive human editing. The combination of the automatic picking and the constrained inversion dramatically reduces the turnaround time of the processing sequence.

INTRINSIC ANISOTROPY

In the inversion procedure, the anisotropy was ignored, and we call the resulting instantaneous velocity V_0 "isotropic." Under the assumption of vertical transverse isotropy (VTI), the isotropic instantaneous velocity V_0 is related to the true vertical anisotropic velocity V_0^{aniso} by

$$V_0^{\text{aniso}} = \frac{V_0}{\sqrt{1 + 2\delta}}, \qquad (22)$$

where δ is the Thomsen (1986) parameter. Superscript "iso" for the isotropic velocity V_0 is omitted. To estimate the interval values of the intrinsic anellipticity η_n^{int}, we use the inverted instantaneous velocity V_0 and the effective anellipticity η_n^{eff}, picked from the analysis of large-offset moveout.

Following Alkhalifah (1997), the fourth-order average velocity of the anisotropic medium V_4 can be defined as

$$V_4^4(t) = \frac{1}{t}\int_0^t V_0^4(\tau) \cdot [1 + 8\eta^{\text{int}}(t)]d\tau. \qquad (23)$$

Assuming that the intrinsic anellipticity is piecewise-constant on the intervals, we obtain

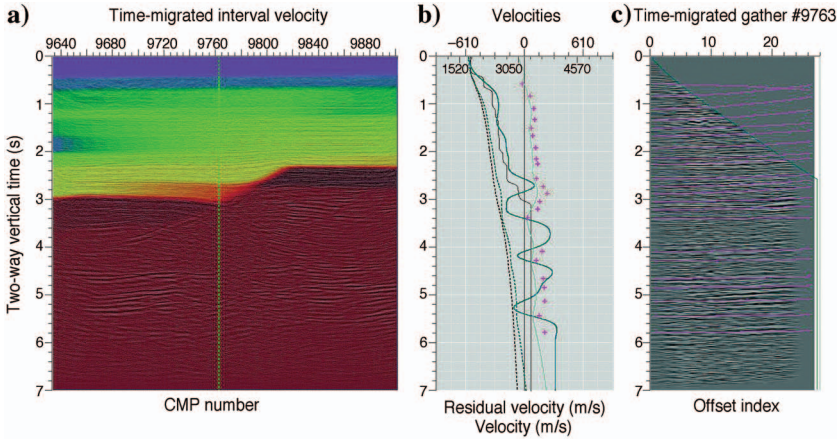

Figure 6. (a) Background-velocity field and results of the PSTM over a fault-shadow region. (b) Results of the inversion for the representative CMP #9763 at the fault. The black solid line is the instantaneous velocity trend $V_0^{\text{trend}}(t)$. Black dashed line is the rms velocity $V_2^{\text{trend}}(t)$ transformed from the velocity trend. The turquoise solid line is the inverted instantaneous velocity V_0^{inv}. The turquoise dashed line is the rms of the inverted velocity V_2^{inv}. The pale blue solid line is the resulting residual rms velocity ΔV_2^{inv}. The pink crosses are the input residual rms velocity $\Delta V_{2,k}^{\text{data}}$. (c) PSTM image gather at CMP #9763. The pink lines are moveout-versus-offset trends for the residual rms velocity picked in Figure 6b (pink crosses).

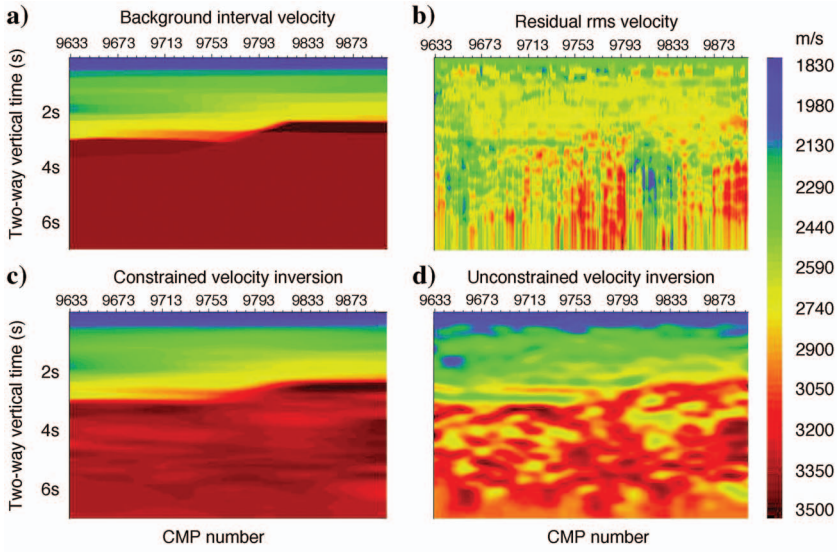

Figure 7. (a) Background instantaneous-velocity field at the fault shadow. The two-way traveltime range is 7 s. (b) Residual rms velocity versus time (input data), obtained by automatic picking. The residual rms-velocity range is -240 m/s $\le \Delta V_2^{\text{Data}} \le 430$ m/s. (c) Results of the constrained velocity inversion. Results are stable and geologically plausible even for a noisy input data set. (d) Results of the unconstrained velocity inversion. Results are somewhat noisy.

$$V_{4,n}^4 \cdot t_n = \sum_{i=1}^{n} (1 + 8\eta_i^{\text{int}}) \cdot \int_{t_{i-1}}^{t_i} V_0^4(\tau) d\tau,$$

$$\Delta t_i = t_i - t_{i-1}, \quad t_n = \sum_{i=1}^{n} \Delta t_i, \quad t_0 = 0. \tag{24}$$

Consider the last interval n connecting interfaces $n-1$ and n. Equation 24 becomes

$$V_{4,n}^4 \cdot t_n - V_{4,n-1}^4 \cdot t_{n-1} = (1 + 8\eta_n^{\text{int}}) \int_{t_{n-1}}^{t_n} V_0^4(\tau) d\tau. \tag{25}$$

Introduce the isotropic nonhyperbolic parameter H_n^{iso} and the anisotropic nonhyperbolic parameter H_n^{aniso} over interval n of the anisotropic medium:

$$H_n^{\text{iso}} = \int_{t_{n-1}}^{t_n} V_0^4(t) dt,$$

$$H_n^{\text{aniso}} = (1 + 8\eta_n^{\text{Int}}) \int_{t_{n-1}}^{t_n} V_0^4(t) dt. \tag{26}$$

Equation 25 relates the anisotropic nonhyperbolic parameter to the fourth-order average velocity $V_{4,n}$ of the anisotropic medium:

$$H_n^{\text{aniso}} = V_{4,n}^4 \cdot t_n - V_{4,n-1}^4 \cdot t_{n-1}. \tag{27}$$

It follows from equation 25 that the intrinsic interval anellipticity depends on the isotropic and the anisotropic nonhyperbolic parameters over the interval,

$$H_n^{\text{aniso}} = (1 + 8\eta_n^{\text{int}}) H_n^{\text{iso}} \rightarrow \eta_n^{\text{int}} = \frac{H_n^{\text{aniso}} - H_n^{\text{iso}}}{8H_n^{\text{iso}}}. \tag{28}$$

In the anisotropic model, the fourth-order average velocity $V_{4,n}$ and the rms velocity $V_{2,n}$ are related by the effective anellipticity η_n^{eff},

$$V_{4,n}^4 = V_{2,n}^4 \cdot (1 + 8\eta_n^{\text{eff}}). \tag{29}$$

Combining equations 27 and 29, we relate the anisotropic nonhyperbolic parameter to the rms velocities and to the effective anellipticities at the ends of the interval:

$$H_n^{\text{aniso}} = V_{2,n}^4 \cdot (1 + 8\eta_n^{\text{eff}}) \cdot t_n - V_{2,n-1}^4 \cdot (1 + 8\eta_{n-1}^{\text{eff}}) \cdot t_{n-1}. \tag{30}$$

To suppress random errors, we average the intrinsic anellipticity within the formation subvolumes. We also calculate the standard deviation of η_n^{int} for each formation to estimate the reliability of the results.

Thus, the algorithm is as follows:

- Calculate the rms velocities from the inverted instantaneous velocities.
- Scan and pick the nodal values of effective anellipticity η_n^{eff} using the fourth-order moveout equation (Alkhalifah and Tsvankin, 1995),

$$t_n^2 = t_{0,n}^2 + \frac{x^2}{V_{2,n}^2} - \frac{2\eta_n^{\text{eff}} x^4}{V_{2,n}^2[V_{2,n}^2 t_{0,n}^2 + (1 + 2\eta_n^{\text{eff}}) x^2]}, \tag{31}$$

  where x is the offset, $t_{0,n}$ is the vertical traveltime, and t_n is the nonvertical traveltime.
- Calculate the anisotropic nonhyperbolic parameter H_n^{aniso} by equation 30. Note that the nodal values of the rms velocities $V_{2,n}$ are obtained by forward Dix transform from the inverted instantaneous velocity $V_{0,n}^{\text{inv}}$ and correspond to a geologically plausible model.
- Calculate the isotropic parameter H_n^{iso} by equation 26.
- Estimate the intrinsic anellipticity by equation 28.
- Average the intrinsic interval anellipticity within the formation.

Equation 28 may be presented in an equivalent form that gives a better insight on the relation between the intrinsic, induced, and effective anellipticities. The induced anellipticity is caused solely by vertical variations of the instantaneous velocity, without accounting for the intrinsic anisotropy of the medium. In the isotropic model, only the induced counterpart η_n^{ind} is present, and equation 30 comes to

$$H_n^{\text{iso}} = V_{2,n}^4 \cdot (1 + 8\eta_n^{\text{ind}}) \cdot t_n - V_{2,n-1}^4 \cdot (1 + 8\eta_{n-1}^{\text{ind}}) \cdot t_{n-1}. \tag{32}$$

Equation 32 can be considered as a definition of the induced anellipticity. At the origin $t_0 = 0$, the induced anellipticity can be assumed to be zero because at this point the rms velocity and the fourth-order average velocity both coincide with the instantaneous velocity. At other nodes equation 32 yields

$$\eta_n^{\text{ind}} = \frac{\sum_{i=1}^{n} H_i^{\text{iso}} - V_{2,n}^4 \cdot t_n}{8V_{2,n}^4 \cdot t_n}. \tag{33}$$

The effective anellipticity includes the intrinsic and the induced components, but it is not a simple sum of these components. Moreover, the induced and the effective anellipticities are nodal values, but the intrinsic anellipticity is an interval value.

Recall that the resulting rms velocities are obtained by the forward Dix transform from the instantaneous velocity model, which, in turn, was obtained from the input rms velocities. The resulting rms velocities are the same for the isotropic model and for the model that takes into account Thomsen parameter δ. Indeed, on the inverse Dix transform, we divide the isotropic instantaneous velocity by the factor $\sqrt{1 + 2\delta}$ to get the true vertical velocity of the anisotropic model. However, on the forward Dix transform that follows the inversion, we multiply the instantaneous velocity by the same factor.

Introducing equations 30 and 32 into equation 28, we obtain

$$\eta_n^{\text{int}} = \frac{V_{2,n}^4(\eta_n^{\text{eff}} - \eta_n^{\text{ind}}) \cdot t_n - V_{2,n-1}^4(\eta_{n-1}^{\text{eff}} - \eta_{n-1}^{\text{ind}}) \cdot t_{n-1}}{V_{2,n}^4 \cdot (1 + 8\eta_n^{\text{ind}}) \cdot t_n - V_{2,n-1}^4 \cdot (1 + 8\eta_{n-1}^{\text{ind}}) \cdot t_{n-1}}. \tag{34}$$

As we see, the intrinsic anisotropy is a function of the difference between the effective and the induced anellipticity. The first Thomsen anisotropy parameter δ is not needed to establish the intrinsic anisotropy. Note that the only noisy component in equation 34 is the effec-

tive anellipticity η_n^{eff}. The rms velocity $V_{2,n}$ and the induced anellipticity η_n^{ind} are obtained solely from the geologically feasible, inverted instantaneous-velocity model. Recall that for the intrinsic anellipticity, subscript n means the number of the interval, whereas for the effective and induced anellipticities, n means the node number.

Parameter η_n^{int} is related to the Thomsen parameters ε and δ,

$$\eta_n^{\text{int}} = \frac{\varepsilon - \delta}{1 + 2\delta}, \quad \varepsilon = \eta_n^{\text{int}} + \delta + 2\eta_n^{\text{int}}\delta. \tag{35}$$

Usually, parameter δ is obtained by correlating seismic traces in the vicinity of the wells to the sonic logs (or from check shots),

$$\delta = \frac{1}{2} \cdot \left[\frac{(V_0^{\text{iso}})^2 \text{ from seismic}}{(V_0^{\text{aniso}})^2 \text{ from well}} - 1 \right], \tag{36}$$

and this makes it possible to estimate ε by equation 35.

LIMITATIONS OF THE METHOD

The proposed approach is a local, 1D inversion in a 3D, laterally varying medium under the assumptions of small offsets and small dips. Under these assumptions, we obtain a stable and geologically plausible initial velocity model, which can be an input for more advanced and powerful methods, such as depth tomography. The motivation for this study is to increase the stability of the Dix-based inversion, with a controlled loss of accuracy. In other words, the aim is to develop a stable and not necessarily accurate approach that gives an initial estimate for the instantaneous-velocity field from rms-velocity data. The main idea is to find a geologically constrained, instantaneous-velocity field that best fits rms-velocity data in a least-squares sense. It is an attractive replacement for the standard, conventional Dix inversion formula.

CONCLUSIONS

We derived a method to estimate nonoscillatory and geologically plausible instantaneous velocities from conventional stacking- or rms-velocity estimates using a combination of geologically credible, internal, analytical trend function and a least-squares fit. A new, stable velocity-inversion algorithm is introduced, especially suitable for compacted-sediment regions, with the ability to handle different types of velocity anomalies. The method is extended for using any arbitrary, external velocity-trend function and, therefore, can also be applied to update background-velocity models with residual rms velocities or residual moveouts. The input data can be located spatially sparse and irregularly.

The inverted instantaneous velocity approximately matches the transformed input rms velocity (in the least-squares sense) and is controlled by the trend function and the antioscillatory damping mechanism. The damping mechanism keeps unwanted vertical oscillations small. The constrained inversion can be combined with automatic picking procedures, resulting in a considerable speed-up of the velocity updating. Automatic picking normally results in noisy data, owing to the complex nature of the seismic data. The field example presented in this study shows that even in the case of a noisy data set, the proposed constrained inversion produces a stable velocity field. The gridding procedure provides further lateral smoothing on a fine, regular grid in both lateral and vertical directions.

On the basis of the reliable, inverted instantaneous-velocity model, it becomes possible to determine intrinsic and induced anisotropy parameters.

LIST OF SYMBOLS

A = Misfit of exponential velocity distribution
B = Data misfit
C = Trend-function misfit
C_i = Spring stiffness
d = Lateral distance between grid node and location of vertical function
D = Damping energy
D_C = Cylindrical stiffness of plate
F = Inversion cost function
G = Inversion gradient
h = Offset
H = Inversion Hessian matrix
H_n^{aniso} = Anisotropic nonhyperbolic parameter for interval n
H_n^{iso} = Isotropic nonhyperbolic parameter for interval n
k_a = Initial gradient of exponential distribution
k_n = Constant gradient on interval n for linear velocity distribution in depth
L_2 = Euclidean norm
M_A = Arithmetic average
M_L = Logarithmic average
N = Amount of nodes in vertical function
p = Pressure applied to a plate surface
R = Radius of influence for internal trend estimate
s = Step of steepest descent
t_H = One-way time for redatum horizon
t_n = One-way vertical time at the bottom interface of layer n
t_{n-1} = One-way vertical time at the top interface of layer n
U_k^{data} = Local rms velocity of input data on interval k between two picked points
U_k^{trend} = Local rms velocity of trend function on interval k between two picked points
U_n = Local rms velocity on interval n
U_n^{lin} = Local rms velocity of linear distribution in depth on interval n
V_a = Initial velocity of exponential distribution
$V_{\text{int},k}^{\text{trend}}$ = Interval velocity of trend on interval k between two picked points
V_n^{int} = Interval (local average) velocity on a regular interval n
V_0^{aniso} = True vertical anisotropic velocity (of compression wave)
$V_{0,k}^{\text{data}}(t)$ = Instantaneous velocity of updated trend (result of unconstrained inversion) on interval k
$V_{0,k}^{\text{trend}}(t)$ = Instantaneous velocity of trend on interval k
$V_{0,n}$ = Instantaneous velocity at node n
V_2^{exp} = rms velocity of exponential distribution
$V_{2,H}$ = rms velocity of redatum horizon
$V_{2,in}^{\text{data}}$ = Regularized input rms velocity for node n of vertical function i

$V_{2,k}^{\text{data}}$ = Input rms velocity at picked point k
$V_{2,k}^{\text{trend}}$ = rms velocity of trend function at picked point k
$V_{2,n}$ = rms velocity at node n
$V_{4,n}$ = Fourth-order average velocity at node n
V_{∞} = Asymptotic velocity of exponential distribution
w = Bending displacement of thin plate
w_{ij}^{L} = Lateral weight for vertical function i and grid node j
w_n^{damp} = Damping weight for joint n
w_n^{rms} = Weight of data misfit on interval n
w_n^{trend} = Weight of trend misfit on interval n
W_k^{data} = Hyperbolic parameter of input data for interval k between picked points
W_k^{trend} = Hyperbolic parameter for background velocity distribution on this interval
W_n = Hyperbolic parameter over interval n
$\hat{z}$ = Distance measured from the top interface of an interval
δ = First Thomsen anisotropy parameter
δU = Uncertainty of local rms velocity
δV_2 = Uncertainty of global rms velocity
Δt_n = One-way layer traveltime
ΔV = Velocity range of exponential distribution
$\Delta V_{0,k}$ = Residual instantaneous velocity on interval k between two picked points
$\Delta V_{2,k}$ = Residual rms velocity at picked point k
Δz_k = Layer thickness corresponding to the true velocity
$\Delta z_k^{\text{trend}}$ = Layer thickness corresponding to velocity of trend in the unconstrained inversion
ε = Second Thomsen anisotropy parameter
η = Anisotropic anellipticity
η_n^{eff} = Effective anellipticity at node n
η_n^{ind} = Induced anellipticity at node n
η_n^{int} = Intrinsic anellipticity on interval n
ν = Poisson's ratio
τ = One-way time measured from the top interface of an interval

ACKNOWLEDGMENTS

We are grateful to our colleague, Dan Kosloff, for fruitful theoretical discussions and valuable comments that clarified the numerical formulation. Special thanks to Dror Meirovich for the assistance in the software development and helpful discussions. Gratitude is extended to the reviewers from Geophysics for numerous constructive remarks and suggestions that helped improve the content and the style of this paper. We thank Paradigm Geophysical for the financial and technical support of this study.

APPENDIX A

UNCERTAINTY OF UNCONSTRAINED INVERSION

In this appendix, we cite two papers to show that the unconstrained Dix inversion may lead to vertical oscillations of the instantaneous velocity and to demonstrate that the uncertainties of the rms velocities are significantly amplified by the inversion, leading to strong uncertainties of the interval velocity. To be consistent with the cited works, the term *interval velocity* is used in this review instead of the more accurate term *local rms velocity* derived by the Dix formula. As we mentioned in the Introduction, there is a negative correlation between the velocity estimates in two successive layers (Landa et al., 1991), which leads to oscillations in the vertical velocity profile. Consider the inverted interval velocity from the Dix equation 1 for the two successive intervals, $\Delta t_n = t_n - t_{n-1}$ and $\Delta t_{n+1} = t_{n+1} - t_n$. Elimination of the rms velocity $V_{2,n}$ at their common interface t_n leads to

$$U_{n+1} = \sqrt{\frac{V_{2,n+1}^2 t_{n+1} - V_{2,n-1}^2 t_{n-1} - U_n^2 \Delta t_n}{\Delta t_{n+1}}},$$

$$\frac{\partial U_{n+1}}{\partial U_n} = -\frac{U_n \Delta t_n}{U_{n+1}\Delta t_{n+1}} \approx -\frac{V_n^{\text{Int}} \Delta t_n}{V_{n+1}^{\text{Int}} \Delta t_{n+1}} = -\frac{\Delta z_n}{\Delta z_{n+1}}. \tag{A-1}$$

Hajnal and Sereda (1981) demonstrated that the uncertainty in the calculated interval velocity increases with depth and is inversely proportional to layer thickness. According to equation A-1, the interval velocity depends on two traveltimes and two rms velocities at the interfaces, and the error of its estimate is

$$\begin{aligned}\delta U_n &= \frac{\partial U_n}{\partial t_n} \cdot \delta t_n + \frac{\partial U_n}{\partial t_{n-1}} \cdot \delta t_{n-1} + \frac{\partial U_n}{\partial V_{2,n}} \cdot \delta V_{2,n} \\ &\quad + \frac{\partial U_n}{\partial V_{2,n-1}} \cdot \delta V_{2,n-1} \\ &= \frac{V_{2,n}^2 - V_{2,n-1}^2}{2\Delta t_n} \cdot \frac{t_n \cdot \delta t_{n-1} - t_{n-1} \cdot \delta t_n}{\sqrt{W_n \cdot \Delta t_n}} \\ &\quad + \frac{V_{2,n} t_n \cdot \delta V_{2,n} - V_{2,n-1} t_{n-1} \cdot \delta V_{2,n-1}}{\sqrt{W_n \cdot \Delta t_n}},\end{aligned} \tag{A-2}$$

where $W_n \equiv V_{2,n}^2 t_n - V_{2,n-1}^2 t_{n-1}$. We call W_n the hyperbolic parameter. Next, note that

$$\frac{V_{2,n}^2 - V_{2,n-1}^2}{2\Delta t_n} \approx \frac{1}{2} \cdot \frac{dV_2^2}{dt} = V_2 \cdot \frac{dV_2}{dt}. \tag{A-3}$$

The right side of equation A-3 is estimated at the midpoint of the interval (for the midpoint, the subscript is omitted). Hajnal and Sereda (1981) assume that the rms velocity varies slowly and neglect the derivative dV_2/dt. Furthermore, they consider the worst case, when the errors of the rms velocities at the top and bottom interface $\delta V_{2,n-1}$ and $\delta V_{2,n}$, respectively, have opposite signs (actually, these signs are unknown). In this case, the error terms $+V_{2,n}t_n \cdot \delta V_{2,n}$ and $-V_{2,n-1}t_{n-1} \cdot \delta V_{2,n-1}$ have the same sign and do not compensate each other. Assuming that the absolute value δV_2 of these errors is the same, the error estimate of the interval velocity becomes

$$\frac{\delta U_n}{\delta V_2} = \frac{V_{2,n}t_n + V_{2,n-1}t_{n-1}}{\sqrt{W_n \cdot \Delta t_n}} \approx \frac{2V_2 t}{\Delta t_n \cdot \sqrt{W_n/\Delta t_n}}$$
$$\approx \frac{2V_2 t/\Delta t_n}{\sqrt{d(V_2^2 t)/dt}} = \frac{2V_2 t/\Delta t_n}{\sqrt{V_2^2 + 2V_2 t \cdot dV_2/dt}} \approx \frac{2t}{\Delta t_n}$$
$$= \frac{t_n + t_{n-1}}{t_n - t_{n-1}}. \qquad \text{(A-4)}$$

The ratio $2t/\Delta t_n$ is the error amplification factor.

APPENDIX B

SOLUTION TECHNIQUE FOR VELOCITY TREND PARAMETERS

The resolving set for minimization of the variation energy follows from equation 9. At the minimum point, these partial derivatives vanish, and the matrix of second derivatives is positive definite:

$$\frac{\partial A_j}{\partial V_{a,j}} = 0, \quad \frac{\partial A_j}{\partial k_{a,j}} = 0. \qquad \text{(B-1)}$$

Subscript j denotes the lateral location. Apply the Newton iterative procedure:

$$\begin{bmatrix} V_{a,j}^{(m+1)} \\ k_{a,j}^{(m+1)} \end{bmatrix} = \begin{bmatrix} V_{a,j}^{(m)} \\ k_{a,j}^{(m)} \end{bmatrix} + \begin{bmatrix} \delta V_{a,j}^{(m)} \\ \delta k_{a,j}^{(m)} \end{bmatrix}, \qquad \text{(B-2)}$$

where m is the number of the current iteration, and $\delta V_{a,j}^{(m)}$ and $\delta k_{a,j}^{(m)}$ are corrections obtained from the linear set,

$$\begin{bmatrix} \frac{\partial^2 A_j}{\partial V_{a,j}^2} & \frac{\partial^2 A_j}{\partial V_{a,j}\,\partial k_{a,j}} \\ \frac{\partial^2 A_j}{\partial V_{a,j}\,\partial k_{a,j}} & \frac{\partial^2 A_j}{\partial k_{a,j}^2} \end{bmatrix} \cdot \begin{bmatrix} \delta V_{a,j}^{(m)} \\ \delta k_{a,j}^{(m)} \end{bmatrix} = - \begin{bmatrix} \frac{\partial A_j}{\partial V_{a,j}} \\ \frac{\partial A_j}{\partial k_{a,j}} \end{bmatrix}. \qquad \text{(B-3)}$$

The first derivatives of the misfit function are

$$\frac{\partial A_j}{\partial V_{a,j}} = \sum_{i=0}^{M_j-1} w_{ij}^L \sum_{n=0}^{N_i} w_n^V \times [V_2^{\exp}(V_{a,j},k_{a,j},t_{in}) - V_{2,in}^{\text{data}}] \cdot \left.\frac{\partial V_2^{\exp}}{\partial V_{a,j}}\right|_{t=t_{in}},$$

$$\frac{\partial A_j}{\partial k_{a,j}} = \sum_{i=0}^{M_j-1} w_{ij}^L \sum_{n=0}^{N_i} w_n^V \times [V_2^{\exp}(V_{a,j},k_{a,j},t_{in}) - V_{2,in}^{\text{data}}] \cdot \left.\frac{\partial V_2^{\exp}}{\partial k_{a,j}}\right|_{t=t_{in}}, \qquad \text{(B-4)}$$

where $V_2^{\exp}(V_{a,j},k_{a,j},t_{in})$ is given by equation 6. The second derivatives of the misfit function are

$$\frac{\partial^2 A_j}{\partial V_{a,j}^2} = \sum_{i=0}^{M_j-1} w_{ij}^L \sum_{n=0}^{N_i} w_n^V \times \left[(V_2^{\exp} - V_{2,in}^{\text{data}}) \cdot \frac{\partial^2 V_2^{\exp}}{\partial V_{a,j}^2} + \left(\frac{\partial V_2^{\exp}}{\partial V_{a,j}}\right)^2 \right],$$

$$\frac{\partial^2 A_j}{\partial k_{a,j}^2} = \sum_{i=0}^{M_j-1} w_{ij}^L \sum_{n=0}^{N_i} w_n^V \times \left[(V_2^{\exp} - V_{2,in}^{\text{data}}) \cdot \frac{\partial^2 V_2^{\exp}}{\partial k_{a,j}^2} + \left(\frac{\partial V_2^{\exp}}{\partial k_{a,j}}\right)^2 \right],$$

$$\frac{\partial^2 A_j}{\partial V_{a,j}\,\partial k_{a,j}} = \sum_{i=0}^{M_j-1} w_{ij}^L \sum_{n=0}^{N_i} w_n^V \times \left[(V_2^{\exp} - V_{2,in}^{\text{data}}) \cdot \frac{\partial^2 V_2^{\exp}}{\partial V_{a,j}\,\partial k_{a,j}} + \frac{\partial V_2^{\exp}}{\partial V_{a,j}} \cdot \frac{\partial V_2^{\exp}}{\partial k_{a,j}} \right]. \qquad \text{(B-5)}$$

In the proximity of the minimum point, the Hessian matrix H (matrix of the second derivatives) is positive definite, and its determinant can not vanish. However, this may happen on the way to the minimum, especially if the initial guess is not very close to the solution. Or, even if the determinant does not vanish, it may become too small — anyway, convergence of the Newton method is not guaranteed for any given initial guess. To overcome this problem, we apply the following algorithm. Before updating the sought parameters, we check whether the value of the cost function at the new point is smaller than its current value. If it is smaller, then we update the parameters and pass to the next iteration. Otherwise, we try to decrease the parameter increments by a factor (we use factor 0.7) and check again. If it does not help, we apply the steepest descent. We try to move in the antigradient direction (with the direction of the gradient established at the current point) and choose the optimal step length. This length is the ratio of two scalars: the gradient length squared over the quadratic norm of the Hessian matrix H and the gradient vector G:

$$s = \frac{G^T \cdot G}{G^T \cdot H \cdot G}, \quad \begin{bmatrix} \delta V_{a,j}^{(m)} \\ \delta k_{a,j}^{(m)} \end{bmatrix} = - sG. \qquad \text{(B-6)}$$

The superscript T indicates a transposed vector. The vector of parameter increments is then the opposite of the gradient multiplied by step. Again, before making a step, we check whether the cost function decreases (because it is not guaranteed that the optimal step is really an optimum). If the function decreases, we proceed. If the function does not decrease, we decrease the length of the step by factor two and check again. If it still does not decrease, we continue decreasing the step. This loop is finite — at some small value of the step, the cost function will necessarily decrease in the antigradient direction. After the antigradient step is done, we immediately return to Newton minimization. Convergence of the steepest descent is very slow, and we use this method only to escape from the ravine point, while continuing further with the Newton method (whose convergence is fast but not guaranteed).

APPENDIX C

TECHNIQUE FOR UNCONSTRAINED INVERSION

In this appendix, we develop the unconstrained inversion procedure that matches the rms-velocity data at the picked points exactly and at the same time follows the velocity-trend model. Assume that on interval k between two successive picked points, the instantaneous velocity follows the velocity-trend function with a constant, residual instantaneous velocity,

$$V_{0,k}^{\text{data}}(t) = V_{0,k}^{\text{trend}}(t) + \Delta V_{0,k}. \tag{C-1}$$

The hyperbolic parameter W_k^{data} of the data between the picked points is calculated as

$$W_k^{\text{data}} = V_{2,k}^2 t_k - V_{2,k-1}^2 t_{k-1}, \tag{C-2}$$

and the following relationship holds:

$$\int_{t_{k-1}}^{t_k} [V_{0,k}^{\text{data}}(\tau)]^2 d\tau \equiv \int_{t_{k-1}}^{t_k} [\, V_{0,k}^{\text{trend}}(\tau) + \Delta V_{0,k}]^2 d\tau = W_k^{\text{data}}. \tag{C-3}$$

Expansion of equation C-3 leads to

$$\int_{t_{k-1}}^{t_k} [V_{0,k}^{\text{trend}}(\tau)]^2 d\tau + 2\Delta V_{0,k} \int_{t_{k-1}}^{t_k} V_{0,k}^{\text{trend}}(\tau) d\tau + \Delta V_{0,k}^2 \Delta t_k = W_k^{\text{data}}, \tag{C-4}$$

where $\Delta t_k = t_k - t_{k-1}$ is the one-way interval traveltime. Equation C-4 can be rearranged in terms of local rms velocity of the trend $U_k^{\text{trend}} = \sqrt{W_k^{\text{trend}}/\Delta t_k}$, local rms velocity of the data $U_k^{\text{data}} = \sqrt{W_k^{\text{data}}/\Delta t_k}$, and the interval (local average) velocity of the trend $V_{\text{Int},k}^{\text{trend}} = \Delta z_k^{\text{trend}}/\Delta t_k$,

$$(U_k^{\text{trend}})^2 \Delta t_k + 2\Delta V_{0,k} \cdot \Delta z_k^{\text{trend}} + \Delta V_{0,k}^2 \Delta t_k = (U_k^{\text{data}})^2 \Delta t_k. \tag{C-5}$$

Divide all terms by traveltime Δt_k,

$$(U_k^{\text{trend}})^2 + 2\,\Delta V_{0,k} V_{\text{int},k}^{\text{trend}} + \Delta V_{0,k}^2 = (U_k^{\text{data}})^2. \tag{C-6}$$

Solving quadratic equation C-6, we obtain the residual of the instantaneous velocity between the picked points

$$\Delta V_{0,k} = \sqrt{(U_k^{\text{data}})^2 - (U_k^{\text{trend}})^2 + (V_{\text{int},k}^{\text{trend}})^2} - V_{\text{int},k}^{\text{trend}}. \tag{C-7}$$

In cases when the local rms velocities of the input data and of the background-trend function, U_k^{data} and U_k^{trend} are close, the expression for a small residual $\Delta V_{0,k}$ can be linearized,

$$\Delta V_{0,k} \approx \frac{(U_k^{\text{data}})^2 - (U_k^{\text{trend}})^2}{2V_{\text{int},k}^{\text{trend}}} = \frac{W_k^{\text{data}} - W_k^{\text{trend}}}{2\Delta z_k^{\text{trend}}}. \tag{C-8}$$

APPENDIX D

VELOCITY VERSUS TIME FOR CONSTANT GRADIENT IN DEPTH

Although the linear velocity distribution in depth (Slotnick, 1936) is very common and widely used, we list here the basic relations for completeness. These relations are used in our inversion algorithm.

Derive the law of the instantaneous velocity in time for constant vertical gradient. We assume a linear distribution of the velocity in depth:

$$V_{0,n}^{\text{lin}}(\hat{z}) = \frac{\Delta z_n - \hat{z}}{\Delta z_n} \cdot V_{0,n-1} + \frac{\hat{z}}{\Delta z_n} \cdot V_{0,n}, \quad \Delta z_n = z_n - z_{n-1}, \tag{D-1}$$

where $V_{0,n-1}$ and $V_{0,n}$ are instantaneous velocities at the top and bottom interface, respectively; Δz_n is the interval thickness; and $0 \le \hat{z} \le \Delta z_n$ is the relative depth measured from the top interface. The one-way interval traveltime is

$$\Delta t_n = \int_0^{\Delta z_n} \frac{d\hat{z}}{V_{0,n}(\hat{z})} = \frac{\Delta z_n}{V_{0,n} - V_{0,n-1}} \cdot \ln \frac{V_{0,n}}{V_{0,n-1}} = \frac{\ln(V_{0,n}/V_{0,n-1})}{k_n}, \tag{D-2}$$

where

$$k_n = \frac{\partial V_{0,n}}{\partial \hat{z}} = \frac{V_{0,n} - V_{0,n-1}}{\Delta z_n} = \text{const} \tag{D-3}$$

is the vertical gradient. Note that the interval (local average) velocity becomes the logarithmic average of the interface velocities,

$$V_{\text{int},n} = \frac{\Delta z_n}{\Delta t_n} = \frac{V_{0,n} - V_{0,n-1}}{\ln(V_{0,n}/V_{0,n-1})} \le \frac{V_{0,n-1} + V_{0,n}}{2}. \tag{D-4}$$

In the case of a linear distribution in depth, the interval velocity never exceeds the average of the interface velocities, and the exact equality in (D-4) occurs only in the case of constant velocity $V_{0,n} = V_{0,n-1}$. According to equation D-2, the velocities at the bottom interface and at any intermediate point of the interval are, respectively,

$$V_{0,n} = V_{0,n-1} \cdot \exp(k_n \Delta t_n), \quad V_{0,n}^{\text{lin}}(\tau) = V_{0,n-1} \cdot \exp(k_n \tau), \tag{D-5}$$

where τ is the one-way traveltime measured from the top interface. We eliminate the gradient k_n from equation set D-5 to get the current instantaneous velocity inside the interval versus interface velocities and time,

$$V_{0,n}^{\text{lin}}(\tau) = V_{0,n-1}^{1-\tau/\Delta t_n} \cdot V_{0,n}^{\tau/\Delta t_n}, \quad 0 \le \tau \le \Delta t_n. \tag{D-6}$$

The logarithm of the velocity becomes

$$\ln V_{0,n}^{\text{lin}}(\tau) = \frac{\Delta t_n - \tau}{\Delta t_n} \cdot \ln V_{0,n-1} + \frac{\tau}{\Delta t_n} \cdot \ln V_{0,n},$$

$$0 \le \tau \le \Delta t_n. \tag{D-7}$$

Compare equations D-1 and D-7. Linear interpolation of the instantaneous velocity in depth means linear interpolation of its logarithm in time. Compute the hyperbolic parameter on the interval,

$$W_n = \int_0^{\Delta t_n} V_{0,n}^2(\tau)\, d\tau = \int_0^{\Delta t_n} V_{0,n-1}^{2\cdot(1-\tau/\Delta t_n)} \cdot V_{0,n}^{2\cdot\tau/\Delta t_n} d\tau$$

$$= \frac{\Delta t_n}{2} \cdot \frac{V_{0,n}^2 - V_{0,n-1}^2}{\ln(V_{0,n}/V_{0,n-1})}. \tag{D-8}$$

The local rms velocity U_n^{lin} on the interval depends only on the velocities at the interfaces:

$$U_n^{\text{lin}} = \sqrt{W_n/\Delta t_n} = \sqrt{\frac{V_{0,n}^2 - V_{0,n-1}^2}{2\ln(V_{0,n}/V_{0,n-1})}}. \tag{D-9}$$

Equation D-9 can be presented as

$$U_n^{\text{lin}} = \sqrt{M_A(V_{0,n-1}, V_{0,n}) \cdot M_L(V_{0,n-1}, V_{0,n})}$$

$$= \sqrt{M_L(V_{0,n-1}^2, V_{0,n}^2)}, \tag{D-10}$$

where M_A and M_L are the arithmetic and logarithmic average of the interface velocities, $M_L \le M_A$. For two positive numbers A and B,

$$M_A(A,B) = \frac{A+B}{2}, \quad M_L = \frac{B-A}{\ln(B/A)}. \tag{D-11}$$

APPENDIX E

SUPPRESSING VERTICAL OSCILLATIONS (DAMPING TECHNIQUE)

In this appendix, we derive the damping terms for two kinds of antioscillatory damping mechanisms: an absolute damping and a damping that follows the velocity trend. For an absolute damping that suppresses any gradient jumps, the corresponding term in the cost function is

$$D = \frac{\overline{V^2\Delta t}}{2} \sum_{n=1}^{N-1} w_n^{\text{damp}} \cdot \Delta t_n \Delta t_{n+1} (k_{n+1} - k_n)^2, \tag{E-1}$$

where n is the number of the joint, and k_{n-1} and k_n are constant gradients for the intervals above and below the joint, respectively. These gradients are obtained from equation D-2,

$$k_{n+1} = \frac{\ln(V_{0,n+1}/V_{0,n})}{\Delta t_{n+1}}, \quad k_n = \frac{\ln(V_{0,n}/V_{0,n-1})}{\Delta t_n}. \tag{E-2}$$

Summation is done over all joints between the interval, i.e., over all nodes, except the first one and the last one. Factor $\overline{V^2\Delta t}$ is a characteristic number to provide proper units. For a uniform, coarse time grid, equation E-1 simplifies to

$$D = \frac{\overline{V^2\Delta t}}{2} \sum_{n=1}^{N-1} w_n^{\text{damp}} \cdot \ln^2\left(\frac{V_{0,n-1} \cdot V_{0,n+1}}{V_{0,n}^2}\right). \tag{E-3}$$

For a damping mechanism whose gradient jumps follow those of the trend,

$$D = \frac{\overline{V^2\Delta t}}{2} \sum_{n=1}^{N-1} w_n^{\text{damp}} \cdot \Delta t_n \Delta t_{n+1} [(k_{n+1} - k_n)$$

$$- (k_{n+1}^{\text{trend}} - k_n^{\text{trend}})]^2. \tag{E-4}$$

For a uniform grid, equation E-4 simplifies to

$$D = \frac{\overline{V^2\Delta t}}{2} \sum_{n=1}^{N-1} w_n^{\text{damp}} \cdot \ln^2\left[\frac{V_{0,n-1} \cdot V_{0,n+1}}{V_{0,n}^2} \cdot \frac{(V_{0,n}^{\text{trend}})^2}{V_{0,n-1}^{\text{trend}} \cdot V_{0,n+1}^{\text{trend}}}\right]. \tag{E-5}$$

A similar damping technique for the Dix velocity inversion was proposed by DuBose (1988), but he assumed a linear velocity variation in time between the nodes. In our model, the velocity between the nodes varies linearly in depth.

APPENDIX F

TECHNIQUE OF CONSTRAINED INVERSION

We compute the derivatives of variation energy with respect to model parameters and set them to zero (Menke, 1989). The cost function F, consisting of rms-fit, trend-fit, and damping terms (B, C, and D, respectively), reaches the minimum value at

$$\frac{\partial F}{\partial V_{0,n}} = \frac{\partial B}{\partial V_{0,n}} + \frac{\partial C}{\partial V_{0,n}} + \frac{\partial D}{\partial V_{0,n}} = 0, \quad n = 0, 1, \ldots, N. \tag{F-1}$$

This is a nonlinear set of $N + 1$ equations. We solve it by the Newton method. First, we get an initial guess for the inverted instantaneous velocities $V_{0,n}^{(0)}$, and then, on each iteration, the corrections are added to the current values $V_{0,n}^{(m)}$,

$$V_{0,n}^{(m+1)} = V_{0,n}^{(m)} + \Delta V_{0,n}^{(m)}, \quad n = 0, 1, \ldots, N. \tag{F-2}$$

To get the corrections $\Delta V_{0,n}$, we solve the linearized set with a pentadiagonal symmetric matrix:

$$\sum_{j=\max(0,n-2)}^{j=\min(N,n+2)} \frac{\partial^2 F}{\partial V_{0,n}\, \partial V_{0,j}} \cdot \Delta V_{0,j} = -\frac{\partial F}{\partial V_{0,n}}. \tag{F-3}$$

Data-misfit and trend-misfit terms of the variation energy are computed for intervals and result in a tridiagonal Hessian matrix. Each component of the damping term is computed for a joint, and thus, the damping mechanism contributes in a pentadiagonal Hessian matrix. One can say that the diagonal components are related to the nodes, the close off-diagonal components are related to the intervals, and the remote off-diagonal components are related to joints.

APPENDIX G

TECHNIQUE OF LATERAL GRIDDING

To map the inverted instantaneous velocity from the lateral locations of vertical functions into a regular lateral grid, we find a surface

of minimum curvature and consider elastic bending of a thin, rectangular plate with free edges resting on springs. The specific surface energy W (per unit area) can be presented as

$$W(x,y) = \frac{D_C}{2} \cdot \left[\underbrace{(w_{xx} + w_{yy})^2}_{\text{Laplacian squared}} - 2(1-\nu) \underbrace{(w_{xx}w_{yy} - w_{xy}^2)}_{\text{Gaussian curvature}} \right], \tag{G-1}$$

where w is the normal displacement and ν is Poisson's ratio. Note that the Gaussian curvature does not contribute to the differential equation. Assume that the cylindrical stiffness of the plate $D_C = 1$. Let p be the normal load (pressure). The variational approach leads to the biharmonic equation

$$\frac{\partial^4 w}{\partial x^4} + 2\frac{\partial^4 w}{\partial x^2\, \partial y^2} + \frac{\partial^4 w}{\partial y^4} = \frac{p}{D_C}. \tag{G-2}$$

We do not solve the differential equation directly, but apply the finite-element method instead. We follow Reddy (1993) and use the standard elements of classical plate theory, nonconformed (CPTN) with three degrees of freedom at each node: normal displacement and its derivatives in x and y. The plate consists of identical rectangular elements, assembled together in a global stiffness matrix. The global nodes are enumerated so that the index runs fast along the shorter side of the plate (this may be either x or y) to keep the bandwidth of the stiffness matrix minimum.

The elastic springs, with stiffness C_i, are attached to the plate at the locations of vertical functions. They are unstretched when the displacements under the springs are equal to the given control values $V_{0,i}$. Actually, this means that external vertical forces are applied at the location of the spring, and their values are $P_i = C_i V_{0,i}$. The point forces are presented by Dirac delta-function δ. The normal pressure in equation G-2 becomes

$$p(x,y) = \sum_{i=1}^{N} \delta(x_i, y_i) \cdot C_i[V_{0,i} - w(x,y)]. \tag{G-3}$$

Note that if the spring is very stiff with respect to the stiffness of the plate, then the external load is balanced mostly by the spring force, and the reaction of the plate will be small. This means that in the case of stiff springs, the displacement under the springs will be almost equal to the value of the control function $V_{0,i}$. If the springs are soft, the solution will be more continuous but less accurate: the resulting displacements at the control points will differ from the control values. The proper choice of the weights is an ad hoc operation and requires trial and error. In addition to control points, we have trend values at all other nodes. They are treated similarly, but trend points have much lesser weights. To assign stiffness of springs, we choose the largest translation element on the diagonal of the stiffness matrix (there are also rotation elements) and consider it as a characteristic translation stiffness of the plate. All elements of the stiffness matrix are proportional to the cylindrical stiffness D_C; therefore, the magnitude of D_C does not matter; one may assume $D_C = 1$. For a fixed D_C, the solution is almost insensitive to Poisson's ratio. Once the characteristic translation stiffness is set, we apply two dimensionless factors: weight of control points (large value) and that of trend points (small value). It is not necessary to set the control data at the nodes; the control points may be inside of rectangular elements. In this case, the scalar load (vertical force) is transformed into 12 components of the load at the nodes, and the scalar spring stiffness is transformed into a 12×12 stiffness matrix. The technique of transform is straightforward: The elastic energy of the scalar spring and that of the spring transformed into a matrix should be the same for equal nodal displacements. The same is true for the work of the external load presented as a scalar point force or as a vector of forces and moments. This makes it possible to process nonnodal vertical functions (a typical case for multiline 2D survey) or to apply the gridding mesh different from the lateral grid of inversion. In addition, the technique allows us to install not only translation springs but also rotation springs, thus to model a control point with given lateral gradients of the velocity. (In the present study this feature is not in use.)

Because, for all horizontal slices, the vertical locations of control points coincide and only the values of control data differ, the global stiffness matrix (that includes both plate and springs) is the same for all slices, and only the external loads differ. Thus, we have to solve many times a linear set with the same symmetric positive definite band matrix and different right-hand sides. We perform only once the square-root decomposition of the stiffness matrix into the identical lower and upper triangular matrices. Then we run the backward substitution for each slice.

APPENDIX H

INVERSION WITH EXTERNAL VELOCITY TREND

As mentioned above, we assume that the inverted instantaneous velocity varies linearly with depth between the nodes of the coarse time grid. When the trend function is specified a priori, we accept the same assumption for the behavior of the trend function between the nodes. The trend velocity is defined by its nodal values, and the nonlinear deviations of the trend function between the nodes are, so far, neglected. Thus, both the instantaneous velocity and its trend are linear in depth (and exponential in time), and this simplifies the computation of the L_2-norm for their difference. Let $V_{0,n-1}$, $V_{0,n}$ be the instantaneous velocities at the upper and lower interfaces of the interval, respectively, and let $V_{0,n-1}^{\text{trend}}$, $V_{0,n}^{\text{trend}}$ be the trend velocities at the same points. At this time, the inverted velocities are unknown and the trend values are known. Between the interfaces, the instantaneous-velocity function and its trend versus depth and time are, respectively,

$$\begin{aligned}
&V_0(\hat{z}) = \frac{\Delta z_n - \hat{z}}{\Delta z_n} \cdot V_{0,n-1} + \frac{\hat{z}}{\Delta z_n} \cdot V_{0,n} && \text{Inverted velocity versus depth}\\
&V_0(\tau) = V_{0,n-1}^{1-\tau/\Delta t_n} \cdot V_{0,n}^{\tau/\Delta t_n} && \text{Inverted velocity versus time}\\
&V_0^{\text{trend}}(\hat{z}) = \frac{\Delta z_n - \hat{z}}{\Delta z_n} \cdot V_{0,n-1}^{\text{trend}} + \frac{\hat{z}}{\Delta z} \cdot V_{0,n}^{\text{trend}} && \text{Trend velocity versus depth}\\
&V_0^{\text{trend}}(\tau) = (V_{0,n-1}^{\text{trend}})^{1-\tau/\Delta t_n} \cdot (V_{0,n}^{\text{trend}})^{\tau/\Delta t_n} && \text{Trend velocity versus time}\\
&0 \le \hat{z} \le \Delta z_n, \quad 0 \le \tau \le \Delta t_n && \text{Depth and time range}
\end{aligned} \tag{H-1}$$

The L_2-norm shows how close the instantaneous velocity is to its trend,

$$L_2 = \int_0^{\Delta t_n} [V_0(\tau) - V_0^{\text{trend}}(\tau)]^2 d\tau \equiv J \cdot \Delta t_n. \quad \text{(H-2)}$$

Relationships from Appendix D lead to

$$J = \frac{V_{0,n}^2 - V_{0,n-1}^2}{2\ln(V_{0,n}/V_{0,n-1})} - \frac{2(V_{0,n}^{\text{trend}} \cdot V_{0,n} - V_{0,n-1}^{\text{trend}} \cdot V_{0,n-1})}{\ln(V_{0,n}/V_{0,n-1}) + \ln(V_{0,n}^{\text{trend}}/V_{0,n-1}^{\text{trend}})} + \frac{(V_{0,n}^{\text{trend}})^2 - (V_{0,n-1}^{\text{trend}})^2}{2\ln(V_{0,n}^{\text{trend}}/V_{0,n-1}^{\text{trend}})}. \quad \text{(H-3)}$$

Using notation for the logarithmic average M_L, we obtain

$$J = M_L(V_{0,n}^2, V_{0,n-1}^2) - 2M_L(V_{0,n}^{\text{trend}} \cdot V_{0,n}, V_{0,n-1}^{\text{trend}} \cdot V_{0,n-1}) + M_L[(V_{0,n}^{\text{trend}})^2, (V_{0,n-1}^{\text{trend}})^2]. \quad \text{(H-4)}$$

The L_2-norm includes three counterparts: the logarithmic average of the inverted velocities squared, the mixed logarithmic average (that of the products $V_{0,n}^{\text{trend}} \cdot V_{0,n}$ and $V_{0,n-1}^{\text{trend}} \cdot V_{0,n-1}$), and the logarithmic average of the trend velocities squared. In other words, there is the inversion counterpart, the mixed counterpart, and the trend counterpart. The trend counterpart $M_L[(V_{0,n}^{\text{trend}})^2, (V_{0,n-1}^{\text{trend}})^2]$ is a constant addition, independent of the inverted velocities, and does not affect the minimization. Introduce the following notations

$$M \equiv M_L(V_{0,n}^2, V_{0,n-1}^2),$$

$$L \equiv M_L(V_{0,n}^{\text{trend}} \cdot V_{0,n}, V_{0,n-1}^{\text{trend}} \cdot V_{0,n-1}). \quad \text{(H-5)}$$

The expressions for the logarithmic average (and its derivatives) can not be used directly when the interface instantaneous velocities $V_{0,n-1}$ and $V_{0,n}$ become equal (zero divide) or when these velocities become very close (insufficient accuracy). However, both numerator and denominator are infinitesimal, and the resulting expressions are finite. The singularity is removable. We expand the ratios into a Taylor series in the neighborhood of the average velocity V_c, to introduce the normalized measure $\tilde{\Delta}$ of the gradient on the interval:

$$V_c \equiv \frac{V_{0,n-1} + V_{0,n}}{2}, \quad \Delta \equiv V_{0,n} - V_{0,n-1}, \quad \tilde{\Delta} \equiv \Delta / V_c. \quad \text{(H-6)}$$

The inversion counterpart becomes

$$\frac{M}{V_c^2} = 1 - \frac{\tilde{\Delta}^2}{12} - \frac{\tilde{\Delta}^4}{180} - \frac{11\tilde{\Delta}^6}{15120} + O(\tilde{\Delta}^8). \quad \text{(H-7)}$$

In the formulas for the mixed counterpart L (equation H-5), the removable singularity arises when the two products of the inverted and trend velocities become equal (or very close): $V_{0,n-1}^{\text{trend}} \cdot V_{0,n-1} \approx V_{0,n}^{\text{trend}} \cdot V_{0,n}$. In this case, we use an expansion similar to equation H-7. Expansions are used when necessary also for derivatives and second derivatives.

Note that the external trend is usually specified at the nodes of the fine time grid, but on the inversion stage, we use only the coarse nodal values of the trend, neglecting the nonlinearities between these nodes. However, the nonlinear component of the trend can be separated and added to the results of the inversion when performing the gridding from the coarse time grid to the fine grid.

REFERENCES

Al-Chalabi, M., 1997a, Instantaneous slowness versus depth functions: Geophysics, **62**, 70–273.

———, 1997b, Parameter nonuniqueness in velocity versus depth functions: Geophysics, **62**, 970–979.

Alkhalifah, T., 1997, Velocity analysis using nonhyperbolic moveout in transversely isotropic media: Geophysics, **62**, 1839–1854.

Alkhalifah, T., and I. Tsvankin, 1995, Velocity analysis for transversely isotropic media: Geophysics, **60**, 1550–1566.

Bhattacharyya, B. K., 1969, Bicubic spline interpolation as a method for treatment of potential field data: Geophysics, **34**, 402–423.

Bishop, T. N., K. P. Bube, R. T. Cutler, R. T. Langan, P. L. Love, J. R. Resnick, R. T. Shuey, D. A. Spindler, and H. W. Wyld, 1985, Tomographic determination of velocity and depth in laterally varying media: Geophysics, **50**, 903–923.

Briggs, I. C., 1974, Machine contouring using minimum curvature: Geophysics, **39**, 39–48.

Deregowski, S. M., 1990, Common offset migration and velocity analysis: First Break, **8**, 225–234.

Dix, C. H., 1955, Seismic velocities from surface measurements: Geophysics, **20**, 68–86.

Druzhinin, A., and A. Hanyga, 1998, Seismic inversion with poor initial guess: Journal of Seismic Exploration, **7**, 29–44.

DuBose, J. B., 1988, A technique for stabilizing interval velocities from the Dix equation: Geophysics, **53**, 1241–1243.

Durbaum, H., 1954, Zur Bestimmung von Wellengeschwindigkeiten aus reflexionsseismischen Messungen: Geophysical Prospecting, **2**, 151–167.

Faust, L. Y., 1951, Seismic velocity as a function of depth and geologic time: Geophysics, **16**, 192–206.

———, 1953, A velocity function including lithologic variation: Geophysics, **18**, 271–288.

Ferguson, R. J., and R. R. Stewart, 1995, Constrained inversion of P-S seismic data: Consortium for Research in Elastic Wave Exploration Seismology (CREWES) Research Report, vol. 7, 18-1–18-12.

Gjoystdal, H., and B. Ursin, 1981, Inversion of reflection times in three dimensions: Geophysics, **46**, 972–973.

Goldin, S. V., 1986, Seismic traveltime inversion: SEG.

Grechka, V. Y., G. A. McMechan, and V. A. Volovodenko, 1996, Solving 1D inverse problems by Chebyshev polynomial expansion: Geophysics, **61**, 1758–1768.

Hajnal, Z., and I. T. Sereda, 1981, Maximum uncertainty of interval velocity estimate: Geophysics, **46**, 1543–1547.

Harlan, W. S., 1999, Constrained Dix inversion: http://billharlan.com/pub/papers/rmsinv.pdf

Hestens, M. R., and E. Stiefel, 1952, Methods of conjugate gradients for solving linear systems: Journal of Research of the National Bureau of Standards, **49**, 409–436.

Houston, C. E., 1939, Seismic paths, assuming a parabolic increase of velocity with depth: Geophysics, **4**, 242–246.

Hubral, P., 1976, Interval velocities from surface measurements in the three-dimensional plane layer case: Geophysics, **41**, 233–242.

Hubral, P., and T. Krey, 1980, Interval velocities from seismic reflection time measurements: SEG.

Kosloff, D., J. Sherwood, Z. Koren, E. Mechet, and Y. Falkovitz, 1996, Velocity and interface depth determination by tomography of depth migrated gathers: Geophysics, **61**, 1511–1523.

Lancaster, P., and K. Salkauskas, 1986, Curve and surface fitting: Academic Press Inc.

Landa, E., D. Kosloff, S. Keydar, Z. Koren, and M. Reshef, 1988, A method for determination of velocity and depth from seismic reflection data: Geophysical Prospecting, **36**, 223–243.

Landa, E., P. Thore, V. Sorin, and Z. Koren, 1991. Interpretation of velocity estimates from coherency inversion: Geophysics, **56**, 1377–1383.

Lines, L. R., and S. Treitel, 1984, A review of least squares inversion and its application to geophysical problems, Tutorial: Geophysical Prospecting, **32**, 159–186.

———, 1985, Inversion with a grain of salt: Geophysics, **50**, 99–109.

Menke, W., 1989, Geophysical data analysis: Discrete inverse theory, revised edition: Academic Press Inc, Harcourt Brace Jovanovich Publishers.

Oldenburg, D. W., S. Levy, and K. Stinson, 1984, Root-mean-square velocities and recovery of the acoustic impedance: Geophysics, **49**, 1653–1663.

Press, W. H., S. A. Teukolsky, W. T. Vetterling, and B. P. Flannery, 1999, Numerical recipes in C: The art of scientific computing: Cambridge University Press.

Ravve, I., and Z. Koren, 2004, Exponential asymptotically bounded velocity model: 74th Annual International Meeting, SEG, Expanded Abstracts, 2435–2438.

———, 2006a, Exponential asymptotically bounded velocity model: Part I — Effective models and velocity transformations: Geophysics, **71**, T53–T65.

———, 2006b, Exponential asymptotically bounded velocity model: Part II

— Ray tracing, Geophysics, **71**, T67–T85.
Reddy, J. N., 1993, Introduction to the finite element analysis: McGraw-Hill.
Ren, J., S. Lee, and R. D. Martinez, 2004, Stable estimation of interval parameters for P-wave pre-stack imaging in VTI media: 66th Conference and Exhibition, EAGE, Extended Abstracts, D047.
Slotnick, M. M., 1936a, On seismic computations, with applications, Part I: Geophysics, **1**, 9–22.
——–, 1936b, On seismic computations, with applications, Part II: Geophysics, **1**, 299–305.
——–, 1959, Lessons in seismic computing: SEG.
Smith, W. H. F., and P. Wessel, 1990, Gridding with continuous curvature splines in tension: Geophysics, **55**, 293–305.
Sorin, V., and A. Hanyga, 1996, Layer velocity estimation: Exploration of model space: Journal of Seismic Exploration, **5**, 245–260.
Stork, C., 1992, Reflection tomography for post-migrated domain: Geophysics, **57**, 680–692.
Swan, H. W., 2001, Velocities from amplitude variation with offset: Geophysics, **66**, 1735–1743.
Tal-Ezer, H., D. Kosloff, and Z. Koren, 1987, An accurate scheme for seismic forward modeling: Geophysical Prospecting, **35**, 479–490.
Taner, M. T., and F. Koehler, 1969, Velocity spectra — Digital computer derivation and applications of velocity functions, Geophysics, **34**, 859–881.
Tarantola, A., 1987, Inverse problem theory: Methods for data fitting and model parameter estimation: Elsevier Science Publishing Co., Inc.
Thomsen, L., 1986, Weak elastic anisotropy: Geophysics, **51**, 1954–1966.
Thore, P., A. Shtuka, M. Lecour, T. Ait-Ettajer, and R. Cognot, 2002, Structural uncertainties: Determination, management, and applications: Geophysics, **67**, 840–852.
Timoshenko, S., and S. Woinowsky-Krieger, 1968, Theory of plates and shells: McGraw Hill.
Toldi, J. L., 1985, Velocity analysis without picking: Ph.D. thesis, Stanford University.
Ursin, B., 1981, Error estimates for inverse modeling schemes using seismic traveltimes: Geophysics, **46**, 1227–1234.
Valenciano, A., M. Brown, A. Guitton, and M. D. Sacchi, 2004, Interval velocity estimation using edge-preserving regularization: 74th Annual International Meeting, SEG, Expanded Abstracts, 2431–2434.
VanDecar, J. C, and R. Snieder, 1994, Obtaining smooth solutions to large, linear, inverse problems: Geophysics, **59**, 818–829.
Vesnaver, A., and G. Bohm, 2000, Staggered or adapted grids for seismic tomography?: The Leading Edge, **19**, 944–950.
Williamson, P. R., 1990, Tomographic inversion in reflection seismology: Geophysical Journal International, **100**, 255–274.
Zhang, L., and Y. Wang, 2003, Integrated velocity inversion and an example of its application: 73rd Annual International Meeting, SEG, Expanded Abstracts, 654–657.